Projected Changes in Mountain Precipitation under CO2-induced warmer climate

Pratik Kad[1], Kyung-Ja Ha[1], Sun-Seon Lee[2], and Jung-Eun Chu[3]

[1]Pusan National University
[2]IBS Center for Climate Physics (ICCP), Pusan National University
[3]City University of Hong Kong

May 8, 2023

Abstract

Mountains play a vital role in shaping regional and global climate, altering atmospheric circulation and precipitation patterns. To this end, identifying projected changes in mountain precipitation is significantly challenging due to topographic complexity. This study explains how mountain precipitation could respond to rising greenhouse gases. Using a series of century-long fully coupled high-resolution simulations conducted with the Community Earth System Model, we aim to disentangle future changes in mountain precipitation in response to atmospheric carbon dioxide (CO2) perturbations. We identify five low-latitude mountain ranges with elevation-dependent precipitation response, including New Guinea, East Africa, Eastern Himalayas, Central America, and Central Andes. Those mountains are expected to have a mixture of increasing and decreasing precipitation in response to CO2-induced warming, especially over the summit and steep topography. To elucidate the mechanisms controlling future changes in mountain precipitation, we propose 'orographic moist-convection feedback' in which an increase in low-level relative humidity enhances local precipitation by strengthening the upward motion through moist processes for the wetting response and vice versa for the drying response. The effects of Mountain precipitation changes can be extended to hydrology and could lead to significant consequences for human societies and ecosystems.

Projected Changes in Mountain Precipitation under CO_2-induced warmer climate

Pratik Kad[1], Kyung-Ja Ha[1,2,3], Sun-Seon Lee[2,4], Jung-Eun Chu[5]

[1]Department of Climate System, Pusan National University, Busan, South Korea

[2]Center for Climate Physics, Institute for Basic Science, Busan, South Korea

[3]BK21 School of Earth and Environmental Systems, Pusan National University, Busan, South Korea

[4]Pusan National University, Busan, South Korea

[5]Low-Carbon and Climate Impact Research Centre, School of Energy and Environment, City University of Hong Kong, Hong Kong, China

Corresponding author: Kyung-Ja Ha (kjha@pusan.ac.kr)

Key Points:

- This study uses a high-resolution model experiment to explain how mountain precipitation could respond to rising atmospheric carbon dioxide (CO2) concentration.
- Projected precipitation changes are dominated over low-latitude mountains, especially the summit and steep topography.
- We propose a mechanism, 'Orographic Moist-Convection feedback', that explains the unprecedented anomalous changes in the mountain climate.

Keywords

Mountain meteorology, elevation-dependent precipitation, CO_2, greenhouse warming, future projection, orographic rainfall.

Abstract

Mountains play a vital role in shaping regional and global climate, altering atmospheric circulation and precipitation patterns. To this end, identifying projected changes in mountain precipitation is significantly challenging due to topographic complexity. This study explains how mountain precipitation could respond to rising greenhouse gases. Using a series of century-long fully coupled high-resolution simulations conducted with the Community Earth System Model, we aim to disentangle future changes in mountain precipitation in response to atmospheric carbon dioxide (CO_2) perturbations. We identify five low-latitude mountain ranges with elevation-dependent precipitation response, including New Guinea, East Africa, Eastern Himalayas, Central America, and Central Andes. Those mountains are expected to have a mixture of increasing and decreasing precipitation in response to CO_2-induced warming, especially over the summit and steep topography. To elucidate the mechanisms controlling future changes in mountain precipitation, we propose 'orographic moist-convection feedback' in which an increase in low-level relative humidity enhances local precipitation by strengthening the upward motion through moist processes for the wetting response and vice versa for the drying response. The effects of Mountain precipitation changes can be extended to hydrology and could lead to significant consequences for human societies and ecosystems.

1 Introduction

Mountains play a significant role in the climate system of the Earth and are an essential part of the global water cycle (Immerzeel et al., 2020; Viviroli et al., 2007). Mountains penetrate deeply into the atmosphere and significantly regulate large-scale circulation (Sandu et al., 2019), such as monsoons, jet streams, storms, and fronts. The increase in warming rate with elevation, referred to as elevation-dependent warming (Kad et al., 2022; N. Pepin et al., 2015; Rangwala & Miller, 2012), is a regional manifestation of greenhouse warming. Additionally, studies on the cryosphere have confirmed that the majority of mountain glaciers are losing their mass (Huss et al., 2017, vol. 5; Immerzeel et al., 2020; Zemp et al., 2019). The Intergovernmental Panel on Climate Change (IPCC) special report on the ocean and the cryosphere in a changing climate confirm that global warming has threatened the mountain system (Hock et al., 2019). However, the IPCC report mainly focuses on the mountain cryosphere, combined with precipitation, snow, permafrost, glaciers, and ice in lakes and rivers. Recent regional changes and an increase in extremes imply a significant change in sediment loads and water quality provided by mountains (Immerzeel et al., 2020; "Mountains of change," 2021). Therefore, understanding local climate change in mountainous regions (Hock et al., 2019; UN, 2015) is crucial for policymakers and stakeholders.

Precipitation over the mountains is driven by the inflow of moisture-laden winds that are lifted as they move over the terrain and condense to form precipitation, warming the atmosphere by latent heat release (Smith, 2018; Wallace & Hobbs, 2006). However, the precipitation response to climate change depends on many other factors (Colle et al., 2013; Smith, 2018), such as the large-scale shifts in atmospheric circulation that can modify moisture transport, affecting regional precipitation(Shi & Durran, 2014, 2015; Siler & Roe, 2014). A study using numerical simulation(Siler & Roe, 2014) found that the increase in precipitation associated with orographic storms on the lee side slope is due to vertical shifts in condensation. A recent study (Tamarin-Brodsky & Hadas, 2019) demonstrated that increased precipitation extremes are triggered by enhanced atmospheric moisture content and upward vertical velocity. Furthermore, remarkable changes in precipitation with respect to elevation during the last few decades have been observed in many regions globally (Napoli et al., 2019; N. C. Pepin et al., 2022; Roe & Baker, 2006; Smith, 2018), typically referred to as the orographic process. Thus far, most of the studies on mountain meteorology underscore the role of extreme events in the mid-latitude environment(Grose et al., 2019; Shi & Durran, 2016, 2015; Siler et al., 2013; Smith, 1979). However, understanding the precipitation and related processes over the mountainous region is restricted, partly due to reliability in precipitation data across mountainous regions (Hock et al., 2019; Zandler et al., 2019) that comes from less spatial coverages of observation stations, the influence of satellite algorithms, and data assimilation schemes (Sun et al., 2018). Therefore, the climate model is a valuable tool for discovering and understanding the physical processes underlying mountain precipitation change.

To account for the complexities above in mountainous precipitation, the scientific community primarily relies on regional climate models as the topographical features still need to be better resolved in the coarse-resolution Global Climate Models (GCMs) (Gutowski et al., 2021).

However, the regional models have limitations in incorporating large-scale features such as the intertropical convergence zone (ITCZ), Madden–Julian Oscillation (MJO), and El Niño–Southern Oscillation (ENSO), and global warming due to their sensitivity to domain size and lateral boundary condition. To overcome this, we adopt an ultra-high-resolution global Earth system model configuration to answer an essential question on how the precipitation over mountainous regions will respond to projected greenhouse gas forcing. The exact impact of CO_2-induced warming on mountain precipitation is complex and can vary depending on the specific conditions of the region. Here, we present a global assessment of future CO_2-induced warming impacts on regional mountains and demonstrate the underlying feedback mechanism.

2 Model Experiment

Ultra-high-resolution simulation strategy

The physical conditions in mesoscale processes, such as moisture advection, atmospheric circulation, and orographic lifting, can significantly affect mountain hydroclimate. Typically, these orographic features are not well resolved in coarse-resolution GCMs, and oftentimes their processes are parameterized (Small et al., 2014). Therefore, an adequate representation of these processes and their future change require a high-resolution climate model (advantages described in ref. Roberts et al., 2018). Hence, we employ a state-of-the-art, ultra-high-resolution, fully coupled climate model, the Community Earth System Model, version 1.2.2 (referred as CESM-UHR, see ref. (Chu et al., 2020) for more details about CESM-UHR experiments and observed biases). The atmospheric component is the Community Atmosphere Model, version 5 (CAM5(Neale et al., 2012)), with a horizontal resolution of about 25 km and 30 vertical layers, allowing realistic regional details such as topography and local processes responsible for orographic processes(Sandu et al., 2019; Small et al., 2014; Tao et al., 2020). The sea surface temperature (SST) boundary conditions in CESM-UHR allows a more realistic representation of the ocean-atmosphere interactions and resolving of mesoscale oceanic features. We conducted a 140-year present-day (PD) simulation using an atmospheric CO_2 concentration of 367 ppm, initialized from a quasi-equilibrated climate state (Small et al., 2014). Two sensitivity experiments were carried out with CO_2 doubling (2×CO_2, 734 ppm) and CO_2 quadrupling (4×CO_2, 1468 ppm) (Chu et al., 2020). Other greenhouse gases have been kept at PD levels in each simulation. Each experiment was branched from the 71st year of the PD experiment and further integrated for 100 model years with prescribed CO_2 concentrations. To investigate the role of greenhouse warming on hydroclimate over mountains, we analyzed the equilibrated last 20 years of each simulation.

3 Methods

Classifying the mountains

Mountains can be classified based on topographic elevation and surface roughness. This study considered a topographic elevation of more than 1 km as a mountain. However, due to the limited horizontal resolution of the model, we were unable to include mountains with a terrain aspect of less than 25 km in our study (e.g., Western Ghats in India, Mt. Kilimanjaro in East Africa, and Highlands in Myanmar).

Vertically integrated moisture flux (kg m^{-1} day^{-1})

The vertically integrated moisture flux (Q) is the horizontal transport of atmospheric moisture by the penetrating winds, as:

$$Q = \frac{1}{g}\int_{1000hPa}^{100hPa} qV\,\partial p$$

where V is horizontal wind velocity, q is specific humidity, g is gravitational constant, and p is the atmospheric pressure.

Vertical cross-sections

Here, we studied the vertical structure to understand the associated processes rather than taking the vertical column average. Either latitude or longitude was chosen for cross-sections in detail based on the change in precipitation and associated vertically integrated moisture advection over the mountain.

Local saturated condensation (g kg^{-1} day^{-1})

Considering that environmental thermodynamics generally follows a moist adiabat, the local saturated condensation rate(Smith, 1979) caused by the adiabatic lifting can be approximated by:

$$c = -\left(\omega_a . \frac{\partial q_s}{\partial p}\right)$$

where ω_a is the ascending vertical velocity, and q_s is the saturated specific humidity.

Saturated specific humidity (g kg^{-1})

Here, we define saturated specific humidity using an empirical method, where saturation vapor pressure (e*) is calculated using the Tetens equation(Murray, 1967).

$$q_s = 0.622\left(\frac{e^*}{p}\right)$$

Static stability (K hPa^{-1})

Static stability is stability of the atmosphere from hydrostatic equilibrium to vertical displacements. We investigated simple static stability using the following equation:

$$s = -\left(\frac{T}{\theta}\right)\left(\frac{\partial \theta}{\partial p}\right)$$

where T is the absolute air temperature and θ is the potential temperature.

Total diabatic heating (K day^{-1})

To understand the heating source in the atmosphere, the total diabatic heating rate(Nigam et al., 2000; Wang et al., 2019) is calculated using the potential temperature, which has conservation properties like those of dry static energy, approximated as:

$$Q_{diabatic} = \frac{T}{\theta}\left(\frac{\partial \theta}{\partial t} + \omega \frac{\partial \theta}{\partial p} + V_h . \nabla \theta\right)$$

where ω is the vertical velocity.

Moist static energy (kJ kg^{-1})

The moist static energy (h) is used as a thermodynamic variable, which represents the addition of dry static energy (DSE, sum of dry air enthalpy and potential energy) and latent static energy (LSE, latent atmospheric heat), as:

$$h = \left(C_p T + gz\right) + \left(L_v q\right)$$

where C_p is specific heat at constant pressure, z is the height above the surface, and L_v is the latent heat of vaporization.

Moisture budget analysis (mm day^{-1})

The vertically integrated moisture budget can be expressed as a linearized equation in terms of precipitation P, where E is evaporation, V is vertical moisture advection and H is horizontal moisture advection. We can neglect the moisture tendency term on the annual time scale, as it's small compared to the rest of terms in the moisture budget (Oueslati et al., 2019):

$$P = E + V + H$$

$$= E - \langle \omega . \frac{\partial q}{\partial p} \rangle - \langle V_h . \nabla q \rangle$$

Consequently, the change in mean precipitation can be expressed as follow:

$$\Delta P = \Delta E + \Delta V + \Delta H$$

Here angle brackets indicate a vertical mass integral, and delta indicates the change in mean state response to CO_2 perturbation of the respective quantity.

Vertical decomposition of moist static energy advection (kJ kg^{-1} day^{-1})

Atmospheric deep convection is mainly constrained by the moist static energy budget(Neelin & Held, 1987) and can be explained using the vertical structure of moist static energy advection. We decomposed vertical moist static energy advection into its dynamic and thermodynamic components.

$$-\Delta\left(\omega . \frac{\partial h}{\partial p}\right) = -\left(\Delta\omega . \frac{\partial \overline{h}}{\partial p}\right) - \left(\overline{\omega} . \frac{\partial \Delta h}{\partial p}\right)$$

$$= dynamic + Therodynamic$$

Quantifying the precipitation extremes

We used the following indices(Karl et al., 1999) to identify projected changes in extreme rainfall events.

The *simple daily intensity index (SDII, mm day*$^{-1}$*)* describes the daily precipitation amount averaged over all wet days in a year. The wet days are when precipitation exceeds more or equals 1 mm day^{-1}. *SDII* is an absolute index used to assess the intensity of extreme precipitation.

The *extreme flooding index (Rx5day, mm)* describes the maximum precipitation amount in five consecutive days. *Rx5day* is generally used to express the changes in likely flood risks, as heavy rain conditions can contribute to flooding conditions over consecutive days.

4 Results and Discussion

Projected elevation-dependent precipitation changes

Generally, the location of the mountain precipitation is determined by local factors (Boos & Pascale, 2021; Smith, 1979, 2018) such as mountain geometry, terrain steepness, surface wind, moisture source, etc. Considering the solidity of mountain geometry, which will not change in the future, changes in surface temperature due to global warming may lead to changes in other factors, such as surface wind and moisture sources. We examine the response of annual mean precipitation to surface local warming (Fig. 1). A global picture of projected temperature changes reveals that mountain systems are susceptible to greenhouse warming (Fig. S1). The response of annual mean precipitation seems more dominant over low-latitudinal mountains (30°S-30°N) as compared to the mountains in high-latitude in the 4×CO_2 experiment (Fig. 1). Strong response in these low-latitude regions can also be linked to the more substantial enhancement of water vapor in the low-latitude than high-latitude and changes in large-scale circulation patterns such as ITCZ(Mamalakis et al., 2021), MJO (Maloney et al., 2019; Roxy et al., 2019), and ENSO (Latif & Keenlyside, 2009; Mamalakis et al., 2021) under greenhouse warming. However, this study emphasizes the regional scale process only because precipitation response is very high over limited areas, implying that changes in regional climate are the dominant factor in the context of mountain precipitation changes. This analysis identifies five mountain regions experiencing significant precipitation changes in response to CO_2 quadrupling. Based on the area that exceeds precipitation response to the local warming by a threshold $\pm$ 0.1 mm/day/°C, we selected the five most prominent regions among the global mountain range: New Guinea, East Africa, Eastern Himalaya, Central America, and Central Andes (Fig. 1a-e). Since the high-resolution simulation can decently capture topographic features, the mean precipitation pattern in the CESM-UHR simulation over mountain ranges seems reliable compared to the CESM-CMIP6 (100 km nominal resolution) (see Fig. S2). The reliability and accuracy of CMIP6 models are restricted due to their utilization of a coarser resolution. However, precipitation biases in CESM-UHR simulation over some regions analogized to satellite observations are very likely due to the model configuration.

The notable changes in precipitation are most likely at high elevations (Fig. S3a-e) under CO_2-induced warming but still are highly uncertain (Hock et al., 2019). Based on the precipitation change over five mountain regions, we define wetting mountains (New Guinea, East Africa, Eastern Himalayas, windward side of Central Andes) where the precipitation increases and drying mountains (Central America, the leeward side of Central Andes) where the precipitation decreases in a CO_2-enriched climate. Interestingly, the spatial pattern of anomalous precipitation over an individual mountain is heterogeneous, predominantly evident at mount summits or steep terrain (Fig. 1), and looks like elevation-dependent precipitation change. The most increase in precipitation intensity is exhibited at Puncak Jaya in New Guinea (Fig. 1a and Fig. S3a). In contrast, there is an overall drying over Central America (Fig. 1d). It should be noted that the highest mountain summit (e.g., Himalayan peaks) experiences inadequate precipitation due to a lack of moisture supply. In such cases (like Eastern Himalaya, Fig. 1c and Fig. S3c), it precipitates over steep topography before reaching the high summit. Central Andes exhibits both responses, wetting over the windward side of Central Andes and drying over the leeward side of Central Andes.

Atmospheric conditions

The moisture advection over the mountains strongly depends on its terrain pattern, which plays an important role in shaping the vertical profile of moisture content and regional atmospheric conditions. The atmospheric relative humidity is assumed to have increased (Tamarin-Brodsky & Hadas, 2019) under a warming scenario through an oceanic pathway, where the Clausius–Clapeyron relation governs the increase in saturation-specific humidity (O'Gorman & Muller, 2010). It is observed that the change in precipitation (Fig. 1) is linked to the vertical structure of the relative humidity (Fig. 2k-o). The major contributor to the precipitation changes is mostly upslope lifting over the mountain terrain (Smith, 1979, 2018; Tao et al., 2020), which change can influence atmospheric humidity and surface wind. The enhancement and reduction of vertical motion are more evident on the mountain summit and slope (Fig. 3). These enhancements are consistently replicated in the 2×CO_2 and 4×CO_2 experiments. Also, updrafts are widespread in the upper level over projected wet (Fig. 2k, l, m, o) and downdrafts over projected drying (Fig. 2n and o) mountains. These results show that moisture influences the vertical motion over mountainous terrain in the projected CO_2-induced warming scenario. The projected precipitation changes in mountain regions are described in terms of the changes in local saturated condensation (Fig. 3), which is a function of saturated humidity and upward vertical velocity. The diabatic heating influences atmospheric stability (black contour in Fig. 4) at the upper level. Fig. 4 highlights the atmospheric stabilization condition. Atmospheric stabilization refers to the resistance of the atmosphere to vertical motion, which can inhibit the development of deep convection, as it makes it harder for air to rise and form deep convection.

Changes in vertical velocity agree well with strengthening moist static energy through latent heat release. A unique core of least moist static energetics can be observed in the vicinity of mountain summits (Fig. 5a-e) in PD climate, which is strengthened in both 2×CO_2 (Fig. 5f-j) and 4×CO_2 experiments (Fig. 5k-o). The atmospheric moist static energy is enhanced overall in a projected CO_2-induced greenhouse warming scenario, followed by lower-level latent static energy. Additionally, precipitation causes additional local moistening and subsequently enhances the latent static energy with a vertical extension of moist static energy (Fig. 5). In drying mountain regions, raised lower-level dry static energy (Fig. 5n, o) can be seen where restricted diabatic surface heating and upper-level cooling (Fig. 4n, o). In addition, we marked an anomalous dry static environment under CO_2 perturbation in these unfavorable regions for upward motion.

Role of moist dynamics

Moisture budget analysis (see Methods and Fig. 6) shows vertical moisture advection has a close relationship with precipitation in the PD and CO_2 experiments (this close relationship can only be found over the wetter area), consistent with previous studies (Oueslati et al., 2019; Yang et al., 2014). Sufficient moisture in the atmospheric column and strong vertical motions resulted in wetting over mountain regions. This framework has been generally utilized to compare local changes in precipitation (Bony et al., 2013; Chou et al., 2012; Huang et al., 2013; Oueslati et al., 2019; Wang et al., 2019). Wetting mountains consistently increase precipitation and vertical moisture advection, whereas drying mountains do not. However, horizontal moisture advection is small compared to vertical moisture advection (Fig. 7). An anomalous increase in moisture advection can be found in the atmosphere over mountains, consistent with precipitation increase, whereas an anomalous decrease in moisture advection with precipitation decrease (Fig. 6 and 7). The moisture advection response (see Supplementary Methods and Fig. S5) is analyzed using vertical moisture advection (in terms of dynamic and thermodynamic components) and horizontal moisture advection. Our results suggest that vertical advection leads to more moisture (Fig. 7), which causes more latent heating, strengthening the upward motion through the thermodynamic factors (Fig. S5) at lower-level closer to the steep mountain terrain. For example, Eastern Himalayas have the thermodynamic component triggered at a lower level from foothills to steep terrain, further reshaping the upper-level dynamic contribution (see Fig. S4h and c). Even though horizontal advection has slight changes over most of the mountains, it plays a crucial role in the windward side of the Central Andes (peripheral to the Pacific Ocean; Fig. 7o and S4o). Using the moist advection approach to understand the seasonal cycle (Fig. 7) and its complexity to explain the observed pattern seems complicated. We endeavored to improve our understanding of the intricate patterns observed in both Central America and the Central Andes using deep convection. Our objective was to gain insights into the multiple factors contributing to the complex patterns observed, including moisture distribution and atmospheric circulation. To achieve this, we studied the role of deep convection and its impact on these patterns.

Atmospheric deep convection

Atmospheric deep convection occurs in the tropics and is mainly associated with vertical motion, causing diabatic heating and moist static energy export (Bui et al., 2016; Neelin & Held, 1987; Yan et al., 2020). Also, as vertical moisture advection plays a dominant role in mountain hydroclimate response to CO_2 quadrupling, we split vertical moist static energy advection into dynamic and thermodynamic components (see Methods). Positive (negative) vertical MSE advection involves the transport of higher (lower) energy in the vertical direction, resulting in an increase (decrease) of available energy in the atmosphere. This can help us explain the respective contribution of energy import or export and its possible linkage to vertical motion. A symmetric pattern (Fig. 8) is observed over mountains with a low-level energy import. Interestingly, this symmetric pattern of moist energetic response shows consistent results with precipitation changes.

In wet regions such as East Africa, the Eastern Himalayas, Central America, and the windward side of Central Andes, there is a positive thermodynamic component in the lower atmosphere (Fig. 8i, m, o) and a negative dynamic component at the upper level (Fig. 8g, h, e). In New Guinea, both thermodynamic and dynamic responses are similar in the lower atmosphere (Fig. 8f and k), which leads to enhanced deep convection and intense precipitation. However, drying mountains have energy imports at lower and upper levels (Fig. 8d, e). At the upper level in Central America and the leeward side of Central Andes, positive dynamic responses (as shown in Fig. 8i and j) impede convection and reduce precipitation. We demonstrated that warming in mountainous areas amplifies the thermodynamic effect (Moustakis et al., 2020) in the lower atmosphere. Based on our analysis, we can infer that the cause of deep convection in wet regions is attributed to the increase in thermodynamic components at a low level and the decrease in dynamic components at the upper level. However, shallow-hinder convection is observed in dry regions due to the increase in the thermodynamic component at a low level and the dynamic component at an upper level.

Orographic moist-convection feedback

An increase in static stability is unfavorable for vertical motion as more upper-level warming will create a more stable troposphere. Several studies (Li & O'Gorman, 2020; Maloney et al., 2019; Sharmila & Walsh, 2018; Shi & Durran, 2015) have shown that global warming leads to increased atmospheric stability, which in turn can cause the atmosphere to become more stratified. Hypothetically, the mountains are supposed to be wetter under a warming scenario, as they can accumulate additional moisture content owing to temperature rise. Similar to conclusions from previous studies (see refs. Li and O'Gorman, 2020; Shi and Durran, 2016, 2015, 2014; Zhao et al., 2020) on the midlatitude mountains, raising moisture in vertical ascending motion results in anomalous diabatic heating through enhanced condensation and triggers precipitation extremes. This anomalous heating is thermodynamically compensated with ascending vertical motion, which sucks moisture from the lower atmosphere (Lau et al., 2020; Tamarin-Brodsky & Hadas, 2019). What determines the precipitation changes over mountains under the future warming climate? We attempted to answer this question by using feedback mechanisms. Herein, we introduce the concept of "Orographic moist-convection" feedback, explaining the loop mechanism in which vertical motion is reshaped by moisture over a mountain in a warming climate that can further amplify or dampen through feedback and vice versa (schematically illustrated in Fig. 9). In response to CO_2 forcing, the wetting mountain regions are found to be associated with wetting response. Wind speed should reduce due to the weaker zonal temperature gradient in warm tropical climates but more moisture gradient (Maloney et al., 2019; Sohn et al., 2019; Vecchi & Soden, 2007). Therefore, a more humid hydroclimate mountain drops the lifted condensation levels. This abundant moisture content elongates the ascending motion by diabatic heating. Precipitation increases are attributed to the wetting response, further amplified by enhanced ascending motion under CO_2 perturbation (Fig. 9a). A substantial increase in diabatic heating leads to deeper vertical heating at upper levels of the atmosphere, supporting deep convection with vertically rising moist static energy from a low level is also favorable for ascending motion. But it coexists with an overall increase in atmospheric stability in the background, which shows this increase in stability would increase the lapse rate (Fig. S3u-y). Deep moist convection in the mountains can counteract the regional lapse rate within this framework. We confirm that the resultant moist-convection feedback appears positive after compensating with processes. On the other hand, the drying mountains are manifested by the drying response of orographic moist-convection feedback (Fig. 9b). The drying regions experience a decrease in saturated moisture content, which leads to a reduction in upward air movement. This is caused by a diabatic cooling anomaly at a lower level, resulting in shallow convection. As a result, the initial humidity is further decreased. Atmospheric stabilization is a counterpart in both responses to maintain equilibrium within the feedback loop. Low-level relative humidity response shows why the initial trigger in some mountainous areas differs from others, as the response increased nearby wetting mountains and decreased nearby drying mountains (Fig. S6). These results indicate that the orographic moist-convection feedback that modifies regional precipitation is evident. Differences in the strength of the feedback on a regional scale can result in varying precipitation responses.

Extreme event reverberation

Extreme events are strongly associated with a change in the mean climate state. Regional atmospheric conditions and local topography strongly affect these extreme events (Zhang & Liang, 2020). Geographical features concerning topography significantly modulate the spatial changes in extreme events (Herold et al., 2016; Shi & Durran, 2015). Besides, change in the background temperature due to CO_2-induced greenhouse warming also contributes to the variability of extreme precipitation. To further understand the change in extreme events in response to CO_2 quadrupling, we examine extremes (Karl et al., 1999) using absolute precipitation criteria (see Methods and Fig. 10), such as the precipitation intensity (SDII) and extreme flooding events (Rx5day). These events (Fig. 10a-e and Fig. S5a-e) coincide with their mean precipitation changes (Fig. 1a-e and Fig. S5a-e) under CO_2-induced greenhouse gas forcing, increasing the events over New Guinea, East Africa, Eastern Himalaya, mountains part of Central Andes, and decreasing over Central America and leeward side of Central Andes. However, certain extreme events are not related to changes in precipitation mean states, like the highest precipitation in 1-day and 5-day over the Eastern Himalayan region (Fig. S5h and m) and heavy rainy days over the Central Andes (Fig. S5t). These amplified events exceed precipitation anomalies, which further exclusively need to be investigated. Time-dependent indices like heavy rainy days R10, R20 (Fig. S5p-t and S5u-y) concurrently pick through vertical moisture advection (consistent with previous attributional studies (O'Gorman et al., 2021; Oueslati et al., 2019; Zhao et al., 2020)). The consequences of such excessive extremes are responsible for excessive surface runoff (Fig. S3k-o), further exacerbating hazards such as river floods, mountain landslides, and debris flow in the mountains and their surrounding regions (Moustakis et al., 2020). It is possible that the CESM-UHR model may have limitations when simulating extreme precipitation in mountainous regions, as these events are often influenced by complex and localized processes that can be challenging to represent accurately in models.

5 Conclusions

The CESM-UHR provides a valuable opportunity for studying regional climate change in a specific region. In the present study, we employed CESM-UHR to address future changes in precipitation patterns in mountain regions due to increasing CO_2 concentrations in the earth's atmosphere. The five most sensitive mountains in the low latitude, including New Guinea, East Africa, Eastern Himalayas, Central America, and Central Andes, are identified based on precipitation response. A comprehensive feedback framework describes the change in precipitation response to adjustments in the mean state of vertical structure and its related processes. Our study proposes "Orographic moist-convection feedback" for precipitation attributions which appear as positive feedback in the climate system, amplifying an initial state. This feedback consists of two primary net responses, wet and drying responses. In the case of wetting response, the warming-induced moisture addition in the mountain terrain favors a strengthening of ascending motion and anomalous diabatic heating through enhanced precipitation, which further enhances the local build-up of humidity. But, in the case of drying response, the moisture shortage restricts the ascending motion, reducing local precipitation and further reducing the moisture. Orographic moist-convection feedback response to CO_2 perturbations could explain the projected wetting in New Guinea, East Africa, the Eastern Himalayas, the windward side of Central Andes, and projected drying in Central America and the leeward side of Central Andes.

Even though our study concentrates on the mean state changes, the proposed feedback mechanism can potentially improve our comprehension of future changes in mountain precipitation variability from diurnal to interannual timescales. The precipitation changes over the mountains can cause other significant threats, such as mountain-ice melting (Chen et al., 2013), loss and degradation of soil (Borrelli et al., 2020), and biodiversity reduction (Peters et al., 2019; Viviroli et al., 2007), which pose severe consequences to humans and the entire our ecosystem (Conway et al., 2019; Elsen et al., 2020). Thus, climate change-induced regional hydroclimatic changes pose formidable challenges to decision-makers in ensuring mountain water management and resilience. The scientific community can apply this framework to investigate the potential threats to water resource management and related biodiversity. Policymakers need to adopt strategic planning risk mitigation related to the mountains and regions highly dependent on mountain resources.

Acknowledgments

The authors wish to acknowledge the use of the PyFerret program for analysis and graphics in this paper. PyFerret is a product of NOAA's Pacific Marine Environmental Laboratory (Information is available at https://ferret.pmel.noaa.gov/Ferret/). The Earth system model used in our study is the Community Earth System Model version 1.2.2 (CESM1.2.2) developed at the National Center for Atmospheric Research. The source code for CESM releases is distributed through a public subversion code repository, CESM1.2 release page is https://www2.cesm.ucar.edu/models/cesm1.2/. The simulations were conducted on the IBS/ICCP supercomputer "Aleph" 1.43 petaflops high-performance Cray XC50-LC Skylake computing system with 18,720 processor cores, 9.59 petabytes storage, and 43 petabytes tape archive space. With heartfelt appreciation, PK acknowledges Axel Timmermann for their invaluable contributions during the initial discussion, which played a crucial role in shaping the content of this work. Authors to extend sincere appreciation to Jahfer Sharif for proofreading and suggestions.

Funding

PK was supported by the National Research Foundation of Korea (NRF) grant funded by the Korean government (MSIT) (Grant No. 2020R1A2C2006860). KH and SL were supported by the Institute for Basic Science (IBS-R028-D1).

Open Research

All data used in this study are publicly available.

The CESM1.2.2 model simulation data are available at https://ibsclimate.org/research/ultra-high-resolution-climate-simulation-project.

The satellite 3B43 dataset was obtained from the Tropical Rainfall Measurement Mission (TRMM, http://doi.org/10.5067/TRMM/TMPA/MONTH/7).

CESM2 model simulation data available at Coupled Model Intercomparison Project Phase 6 (CMIP6) provided by ESGF link (https://esgf-node.llnl.gov/projects/cmip6/). Users should select the source id as CESM2.

Author Contributions

PK and KH conceived the study and wrote the initial manuscript draft. PK performed the analysis and investigation and prepared all the figures. SL conducted the model simulations. JC assisted in model data extraction. All authors interpreted the results and contributed to improving the final manuscript.

References

Bony, S., Bellon, G., Klocke, D., Sherwood, S., Fermepin, S., & Denvil, S. (2013). Robust direct effect of carbon dioxide on tropical circulation and regional precipitation. *Nature Geoscience*, *6*(6). https://doi.org/10.1038/ngeo1799

Boos, W. R., & Pascale, S. (2021). Mechanical forcing of the North American monsoon by orography. *Nature*, *599*(7886), 611–615. https://doi.org/10.1038/s41586-021-03978-2

Borrelli, P., Robinson, D. A., Panagos, P., Lugato, E., Yang, J. E., Alewell, C., et al. (2020). Land use and climate change impacts on global soil erosion by water (2015-2070). *Proceedings of the National Academy of Sciences of the United States of America*, *117*(36). https://doi.org/10.1073/pnas.2001403117

Bui, H. X., Yu, J. Y., & Chou, C. (2016). Impacts of vertical structure of large-scale vertical motion in tropical climate: Moist static energy framework. *Journal of the Atmospheric Sciences*, *73*(11). https://doi.org/10.1175/JAS-D-16-0031.1

Chen, J. L., Wilson, C. R., & Tapley, B. D. (2013). Contribution of ice sheet and mountain glacier melt to recent sea level rise. *Nature Geoscience*, *6*(7). https://doi.org/10.1038/ngeo1829

Chou, C., Chen, C. A., Tan, P. H., & Chen, K. T. (2012). Mechanisms for global warming impacts on precipitation frequency and intensity. *Journal of Climate*, *25*(9), 3291–3306. https://doi.org/10.1175/JCLI-D-11-00239.1

Chu, J.-E., Lee, S.-S., Timmermann, A., Wengel, C., Stuecker, M. F., & Yamaguchi, R. (2020). Reduced tropical cyclone densities and ocean effects due to anthropogenic greenhouse warming. *Science Advances*, *6*(51), eabd5109. https://doi.org/10.1126/sciadv.abd5109

Colle, B. A., Smith, R. B., & Wesley, D. A. (2013). Theory, Observations, and Predictions of Orographic Precipitation. https://doi.org/10.1007/978-94-007-4098-3_6

Conway, D., Nicholls, R. J., Brown, S., Tebboth, M. G. L., Adger, W. N., Ahmad, B., et al. (2019). The need for bottom-up assessments of climate risks and adaptation in climate-sensitive regions. *Nature Climate Change*, *9*(7). https://doi.org/10.1038/s41558-019-0502-0

Elsen, P. R., Monahan, W. B., & Merenlender, A. M. (2020). Topography and human pressure in mountain ranges alter expected species responses to climate change. *Nature Communications*, *11*(1). https://doi.org/10.1038/s41467-020-15881-x

Grose, M. R., Syktus, J., Thatcher, M., Evans, J. P., Ji, F., Rafter, T., & Remenyi, T. (2019). The role of topography on projected rainfall change in mid-latitude mountain regions. *Climate Dynamics*, *53*(5–6). https://doi.org/10.1007/s00382-019-04736-x

Gutowski, W. J., Ullrich, P. A., Hall, A., Leung, L. R., O'Brien, T. A., Patricola, C. M., et al. (2021). The ongoing need for high-resolution regional climate models: Process understanding and stakeholder information. *Bulletin of the American Meteorological Society*, *101*(5). https://doi.org/10.1175/BAMS-D-19-0113.1

Herold, N., Alexander, L. v., Donat, M. G., Contractor, S., & Becker, A. (2016). How much does it rain over land? *Geophysical Research Letters*, *43*(1). https://doi.org/10.1002/2015GL066615

Hock, R., Rasul, G., Adler, C., Cáceres, B., Gruber, S., Hirabayashi, Y., et al. (2019). Chapter 2: High Mountain Areas. IPCC Special Report on the Ocean and Cryosphere in a Changing Climate. In *IPCC Special Report on the Ocean and Cryosphere in a Changing Climate*.

Huang, P., Xie, S. P., Hu, K., Huang, G., & Huang, R. (2013). Patterns of the seasonal response of tropical rainfall to global warming. *Nature Geoscience*, *6*(5). https://doi.org/10.1038/ngeo1792

Huss, M., Bookhagen, B., Huggel, C., Jacobsen, D., Bradley, R. S., Clague, J. J., et al. (2017). Toward mountains without permanent snow and ice. *Earth's Future*, *5*(5), 418–435. https://doi.org/10.1002/2016EF000514

Immerzeel, W. W., Lutz, A. F., Andrade, M., Bahl, A., Biemans, H., Bolch, T., et al. (2020). Importance and vulnerability of the world's water towers. *Nature*, *577*(7790), 364–369. https://doi.org/10.1038/s41586-019-1822-y

Kad, P., Blau, M. T., Ha, K.-J., & Zhu, J. (2022). Elevation-dependent temperature response in early Eocene using paleoclimate model experiment. *Environmental Research Letters*, *17*(11), 114038. https://doi.org/10.1088/1748-9326/ac9c74

Karl, T. R., Nicholls, N., & Ghazi, A. (1999). CLIVAR/GCOS/WMO Workshop on Indices and Indicators for Climate Extremes - Workshop summary. In *Climatic Change* (Vol. 42). https://doi.org/10.1023/A:1005491526870

Latif, M., & Keenlyside, N. S. (2009). El Niño/Southern Oscillation response to global warming. *Proceedings of the National Academy of Sciences of the United States of America*, *106*(49). https://doi.org/10.1073/pnas.0710860105

Lau, W. K. M., Kim, K. M., Chern, J. D., Tao, W. K., & Leung, L. R. (2020). Structural changes and variability of the ITCZ induced by radiation–cloud–convection–circulation interactions: inferences from the Goddard Multi-scale Modeling Framework (GMMF) experiments. *Climate Dynamics*, *54*(1–2). https://doi.org/10.1007/s00382-019-05000-y

Li, Z., & O'Gorman, P. A. (2020). Response of vertical velocities in extratropical precipitation extremes to climate change. *Journal of Climate*, *33*(16). https://doi.org/10.1175/JCLI-D-19-0766.1

Maloney, E. D., Adames, Á. F., & Bui, H. X. (2019). Madden–Julian oscillation changes under anthropogenic warming. *Nature Climate Change*. https://doi.org/10.1038/s41558-018-0331-6

Mamalakis, A., Randerson, J. T., Yu, J. Y., Pritchard, M. S., Magnusdottir, G., Smyth, P., et al. (2021). Zonally contrasting shifts of the tropical rain belt in response to climate change. *Nature Climate Change*, *11*(2). https://doi.org/10.1038/s41558-020-00963-x

Mountains of change. (2021). *Nature Geoscience*, *14*(2), 57–57. https://doi.org/10.1038/s41561-021-00694-4

Moustakis, Y., Onof, C. J., & Paschalis, A. (2020). Atmospheric convection, dynamics and topography shape the scaling pattern of hourly rainfall extremes with temperature globally. *Communications Earth & Environment*, *1*(1). https://doi.org/10.1038/s43247-020-0003-0

Murray, F. W. (1967). On the Computation of Saturation Vapor Pressure. *Journal of Applied Meteorology*, *6*(1). https://doi.org/10.1175/1520-0450(1967)006<0203:otcosv>2.0.co;2

Napoli, A., Crespi, A., Ragone, F., Maugeri, M., & Pasquero, C. (2019). Variability of orographic enhancement of precipitation in the Alpine region. *Scientific Reports*, *9*(1). https://doi.org/10.1038/s41598-019-49974-5

Neale, R. B., Gettelman, A., Park, S., Chen, C., Lauritzen, P. H., Williamson, D. L., et al. (2012). Description of the NCAR Community Atmosphere Model (CAM 5.0). NCAR Technical Notes. *Ncar/Tn-464+Str*.

Neelin, J. D., & Held, I. M. (1987). Modeling tropical convergence based on the moist static energy budget. *Monthly Weather Review*, *115*(1). https://doi.org/10.1175/1520-0493(1987)115<0003:MTCBOT>2.0.CO;2

Nigam, S., Chung, C., & DeWeaver, E. (2000). ENSO diabatic heating in ECMWF and NCEP-NCAR reanalyses, and NCAR CCM3 simulation. *Journal of Climate*, *13*(17). https://doi.org/10.1175/1520-0442(2000)013<3152:EDHIEA>2.0.CO;2

O'Gorman, P. A., & Muller, C. J. (2010). How closely do changes in surface and column water vapor follow Clausius-Clapeyron scaling in climate change simulations? *Environmental Research Letters*, *5*(2). https://doi.org/10.1088/1748-9326/5/2/025207

O'Gorman, P. A., Li, Z., Boos, W. R., & Yuval, J. (2021). Response of extreme precipitation to uniform surface warming in quasi-global aquaplanet simulations at high resolution. *Philosophical Transactions of the Royal Society A: Mathematical, Physical and Engineering Sciences*, *379*(2195). https://doi.org/10.1098/rsta.2019.0543

Oueslati, B., Yiou, P., & Jézéquel, A. (2019). Revisiting the dynamic and thermodynamic processes driving the record-breaking January 2014 precipitation in the southern UK. *Scientific Reports*, *9*(1). https://doi.org/10.1038/s41598-019-39306-y

Pepin, N., Bradley, R. S., Diaz, H. F., Baraer, M., Caceres, E. B., Forsythe, N., et al. (2015). Elevation-dependent warming in mountain regions of the world. *Nature Climate Change*. https://doi.org/10.1038/nclimate2563

Pepin, N. C., Arnone, E., Gobiet, A., Haslinger, K., Kotlarski, S., Notarnicola, C., et al. (2022). Climate Changes and Their Elevational Patterns in the Mountains of the World. *Reviews of Geophysics*, *60*(1). https://doi.org/10.1029/2020rg000730

Peters, M. K., Hemp, A., Appelhans, T., Becker, J. N., Behler, C., Classen, A., et al. (2019). Climate–land-use interactions shape tropical mountain biodiversity and ecosystem functions. *Nature*, *568*(7750). https://doi.org/10.1038/s41586-019-1048-z

Rangwala, I., & Miller, J. R. (2012). Climate change in mountains: A review of elevation-dependent warming and its possible causes. *Climatic Change*, *114*(3–4). https://doi.org/10.1007/s10584-012-0419-3

Roberts, M. J., Vidale, P. L., Senior, C., Hewitt, H. T., Bates, C., Berthou, S., et al. (2018). The benefits of global high resolution for climate simulation process understanding and the enabling of stakeholder decisions at the regional scale. *Bulletin of the American Meteorological Society*, *99*(11). https://doi.org/10.1175/BAMS-D-15-00320.1

Roe, G. H., & Baker, M. B. (2006). Microphysical and geometrical controls on the pattern of orographic precipitation. *Journal of the Atmospheric Sciences*, *63*(3). https://doi.org/10.1175/JAS3619.1

Roxy, M. K., Dasgupta, P., McPhaden, M. J., Suematsu, T., Zhang, C., & Kim, D. (2019). Twofold expansion of the Indo-Pacific warm pool warps the MJO life cycle. *Nature*, *575*(7784). https://doi.org/10.1038/s41586-019-1764-4

Sandu, I., van Niekerk, A., Shepherd, T. G., Vosper, S. B., Zadra, A., Bacmeister, J., et al. (2019). Impacts of orography on large-scale atmospheric circulation. *Npj Climate and Atmospheric Science*, *2*(1). https://doi.org/10.1038/s41612-019-0065-9

Sharmila, S., & Walsh, K. J. E. (2018). Recent poleward shift of tropical cyclone formation linked to Hadley cell expansion. *Nature Climate Change*, *8*(8). https://doi.org/10.1038/s41558-018-0227-5

Shi, X., & Durran, D. (2016). Sensitivities of extreme precipitation to global warming are lower over mountains than over oceans and plains. *Journal of Climate*, *29*(13). https://doi.org/10.1175/JCLI-D-15-0576.1

Shi, X., & Durran, D. R. (2014). The response of orographic precipitation over idealized midlatitude mountains due to global increases in CO2. *Journal of Climate*, *27*(11). https://doi.org/10.1175/JCLI-D-13-00460.1

Shi, X., & Durran, D. R. (2015). Estimating the response of extreme precipitation over midlatitude mountains to global warming. *Journal of Climate*, *28*(10). https://doi.org/10.1175/JCLI-D-14-00750.1

Siler, N., & Roe, G. (2014). How will orographic precipitation respond to surface warming? An idealized thermodynamic perspective. *Geophysical Research Letters*, *41*(7). https://doi.org/10.1002/2013GL059095

Siler, N., Roe, G., & Durran, D. (2013). On the dynamical causes of variability in the rain-shadow effect: A case study of the Washington Cascades. *Journal of Hydrometeorology*, *14*(1). https://doi.org/10.1175/JHM-D-12-045.1

Small, R. J., Bacmeister, J., Bailey, D., Baker, A., Bishop, S., Bryan, F., et al. (2014). A new synoptic scale resolving global climate simulation using the Community Earth System Model. *Journal of Advances in Modeling Earth Systems*, *6*(4). https://doi.org/10.1002/2014MS000363

Smith, R. B. (1979). The influence of mountains on the atmosphere. *Advances in Geophysics*, *21*(C). https://doi.org/10.1016/S0065-2687(08)60262-9

Smith, R. B. (2018). 100 years of progress on mountain meteorology research. *Meteorological Monographs*, *59*. https://doi.org/10.1175/AMSMONOGRAPHS-D-18-0022.1

Sohn, B. J., Yeh, S. W., Lee, A., & Lau, W. K. M. (2019). Regulation of atmospheric circulation controlling the tropical Pacific precipitation change in response to CO 2 increases. *Nature Communications*, *10*(1). https://doi.org/10.1038/s41467-019-08913-8

Sun, Q., Miao, C., Duan, Q., Ashouri, H., Sorooshian, S., & Hsu, K. L. (2018). A Review of Global Precipitation Data Sets: Data Sources, Estimation, and Intercomparisons. *Reviews of Geophysics*, *56*(1). https://doi.org/10.1002/2017RG000574

Tamarin-Brodsky, T., & Hadas, O. (2019). The Asymmetry of Vertical Velocity in Current and Future Climate. *Geophysical Research Letters*, *46*(1). https://doi.org/10.1029/2018GL080363

Tao, W., Huang, G., Lau, W. K. M., Dong, D., Wang, P., & Wen, G. (2020). How can CMIP5 AGCMs' resolution influence precipitation in mountain areas: the Hengduan Mountains? *Climate Dynamics*, *54*(1–2). https://doi.org/10.1007/s00382-019-04993-w

UN. United Nations Transforming Our World: the 2030 Agenda for Sustainable Development. A/RES/70/1, 16301 United Nations § (2015).

Vecchi, G. A., & Soden, B. J. (2007). Global warming and the weakening of the tropical circulation. *Journal of Climate*, *20*(17). https://doi.org/10.1175/JCLI4258.1

Viviroli, D., Dürr, H. H., Messerli, B., Meybeck, M., & Weingartner, R. (2007). Mountains of the world, water towers for humanity: Typology, mapping, and global significance. *Water Resources Research*, *43*(7). https://doi.org/https://doi.org/10.1029/2006WR005653

Wallace, J. M., & Hobbs, P. v. (2006). *Atmospheric Science: An Introductory Survey: Second Edition*. *Atmospheric Science: An Introductory Survey: Second Edition*. https://doi.org/10.1016/C2009-0-00034-8

Wang, M., Wang, J., Duan, A., Yang, J., & Liu, Y. (2019). Quasi-biweekly impact of the atmospheric heat source over the Tibetan Plateau on summer rainfall in Eastern China. *Climate Dynamics*, *53*(7–8). https://doi.org/10.1007/s00382-019-04798-x

Yan, Z., Wu, B., Li, T., Collins, M., Clark, R., Zhou, T., et al. (2020). Eastward shift and extension of ENSO-induced tropical precipitation anomalies under global warming. *Science Advances*, *6*(2). https://doi.org/10.1126/sciadv.aax4177

Yang, Q., Ruby Leung, L., Rauscher, S. A., Ringler, T. D., & Taylor, M. A. (2014). Atmospheric moisture budget and spatial resolution dependence of precipitation extremes in aquaplanet simulations. *Journal of Climate*, *27*(10). https://doi.org/10.1175/JCLI-D-13-00468.1

Zandler, H., Haag, I., & Samimi, C. (2019). Evaluation needs and temporal performance differences of gridded precipitation products in peripheral mountain regions. *Scientific Reports*, *9*(1). https://doi.org/10.1038/s41598-019-51666-z

Zemp, M., Huss, M., Thibert, E., Eckert, N., McNabb, R., Huber, J., et al. (2019). Global glacier mass changes and their contributions to sea-level rise from 1961 to 2016. *Nature*, *568*(7752). https://doi.org/10.1038/s41586-019-1071-0

Zhang, Y., & Liang, C. (2020). Analysis of Annual and Seasonal Precipitation Variation in the Qinba Mountain area, China. *Scientific Reports*, *10*(1). https://doi.org/10.1038/s41598-020-57743-y

Zhao, Y., Chen, D., Li, J., Chen, D., Chang, Y., Li, J., & Qin, R. (2020). Enhancement of the summer extreme precipitation over North China by interactions between moisture convergence and topographic settings. *Climate Dynamics*, *54*(5–6). https://doi.org/10.1007/s00382-020-05139-z

Projected Changes in Mountain Precipitation under CO_2-induced warmer climate

Pratik Kad[1], Kyung-Ja Ha[1,2,3], Sun-Seon Lee[2,4], Jung-Eun Chu[5]

[1]Department of Climate System, Pusan National University, Busan, South Korea

[2]Center for Climate Physics, Institute for Basic Science, Busan, South Korea

[3]BK21 School of Earth and Environmental Systems, Pusan National University, Busan, South Korea

[4]Pusan National University, Busan, South Korea

[5]Low-Carbon and Climate Impact Research Centre, School of Energy and Environment, City University of Hong Kong, Hong Kong, China

Corresponding author: Kyung-Ja Ha (kjha@pusan.ac.kr)

Key Points:

- This study uses a high-resolution model experiment to explain how mountain precipitation could respond to rising atmospheric carbon dioxide (CO2) concentration.
- Projected precipitation changes are dominated over low-latitude mountains, especially the summit and steep topography.
- We propose a mechanism, 'Orographic Moist-Convection feedback', that explains the unprecedented anomalous changes in the mountain climate.

Keywords

Mountain meteorology, elevation-dependent precipitation, CO_2, greenhouse warming, future projection, orographic rainfall.

Abstract

Mountains play a vital role in shaping regional and global climate, altering atmospheric circulation and precipitation patterns. To this end, identifying projected changes in mountain precipitation is significantly challenging due to topographic complexity. This study explains how mountain precipitation could respond to rising greenhouse gases. Using a series of century-long fully coupled high-resolution simulations conducted with the Community Earth System Model, we aim to disentangle future changes in mountain precipitation in response to atmospheric carbon dioxide (CO_2) perturbations. We identify five low-latitude mountain ranges with elevation-dependent precipitation response, including New Guinea, East Africa, Eastern Himalayas, Central America, and Central Andes. Those mountains are expected to have a mixture of increasing and decreasing precipitation in response to CO_2-induced warming, especially over the summit and steep topography. To elucidate the mechanisms controlling future changes in mountain precipitation, we propose 'orographic moist-convection feedback' in which an increase in low-level relative humidity enhances local precipitation by strengthening the upward motion through moist processes for the wetting response and vice versa for the drying response. The effects of Mountain precipitation changes can be extended to hydrology and could lead to significant consequences for human societies and ecosystems.

1 Introduction

Mountains play a significant role in the climate system of the Earth and are an essential part of the global water cycle (Immerzeel et al., 2020; Viviroli et al., 2007). Mountains penetrate deeply into the atmosphere and significantly regulate large-scale circulation (Sandu et al., 2019), such as monsoons, jet streams, storms, and fronts. The increase in warming rate with elevation, referred to as elevation-dependent warming (Kad et al., 2022; N. Pepin et al., 2015; Rangwala & Miller, 2012), is a regional manifestation of greenhouse warming. Additionally, studies on the cryosphere have confirmed that the majority of mountain glaciers are losing their mass (Huss et al., 2017, vol. 5; Immerzeel et al., 2020; Zemp et al., 2019). The Intergovernmental Panel on Climate Change (IPCC) special report on the ocean and the cryosphere in a changing climate confirm that global warming has threatened the mountain system (Hock et al., 2019). However, the IPCC report mainly focuses on the mountain cryosphere, combined with precipitation, snow, permafrost, glaciers, and ice in lakes and rivers. Recent regional changes and an increase in extremes imply a significant change in sediment loads and water quality provided by mountains (Immerzeel et al., 2020; "Mountains of change," 2021). Therefore, understanding local climate change in mountainous regions (Hock et al., 2019; UN, 2015) is crucial for policymakers and stakeholders.

Precipitation over the mountains is driven by the inflow of moisture-laden winds that are lifted as they move over the terrain and condense to form precipitation, warming the atmosphere by latent heat release (Smith, 2018; Wallace & Hobbs, 2006). However, the precipitation response to climate change depends on many other factors (Colle et al., 2013; Smith, 2018), such as the large-scale shifts in atmospheric circulation that can modify moisture transport, affecting regional precipitation(Shi & Durran, 2014, 2015; Siler & Roe, 2014). A study using numerical simulation(Siler & Roe, 2014) found that the increase in precipitation associated with orographic storms on the lee side slope is due to vertical shifts in condensation. A recent study (Tamarin-Brodsky & Hadas, 2019) demonstrated that increased precipitation extremes are triggered by enhanced atmospheric moisture content and upward vertical velocity. Furthermore, remarkable changes in precipitation with respect to elevation during the last few decades have been observed in many regions globally (Napoli et al., 2019; N. C. Pepin et al., 2022; Roe & Baker, 2006; Smith, 2018), typically referred to as the orographic process. Thus far, most of the studies on mountain meteorology underscore the role of extreme events in the mid-latitude environment(Grose et al., 2019; Shi & Durran, 2016, 2015; Siler et al., 2013; Smith, 1979). However, understanding the precipitation and related processes over the mountainous region is restricted, partly due to reliability in precipitation data across mountainous regions (Hock et al., 2019; Zandler et al., 2019) that comes from less spatial coverages of observation stations, the influence of satellite algorithms, and data assimilation schemes (Sun et al., 2018). Therefore, the climate model is a valuable tool for discovering and understanding the physical processes underlying mountain precipitation change.

To account for the complexities above in mountainous precipitation, the scientific community primarily relies on regional climate models as the topographical features still need to be better resolved in the coarse-resolution Global Climate Models (GCMs) (Gutowski et al., 2021).

However, the regional models have limitations in incorporating large-scale features such as the intertropical convergence zone (ITCZ), Madden–Julian Oscillation (MJO), and El Niño–Southern Oscillation (ENSO), and global warming due to their sensitivity to domain size and lateral boundary condition. To overcome this, we adopt an ultra-high-resolution global Earth system model configuration to answer an essential question on how the precipitation over mountainous regions will respond to projected greenhouse gas forcing. The exact impact of CO_2-induced warming on mountain precipitation is complex and can vary depending on the specific conditions of the region. Here, we present a global assessment of future CO_2-induced warming impacts on regional mountains and demonstrate the underlying feedback mechanism.

2 Model Experiment

Ultra-high-resolution simulation strategy

The physical conditions in mesoscale processes, such as moisture advection, atmospheric circulation, and orographic lifting, can significantly affect mountain hydroclimate. Typically, these orographic features are not well resolved in coarse-resolution GCMs, and oftentimes their processes are parameterized (Small et al., 2014). Therefore, an adequate representation of these processes and their future change require a high-resolution climate model (advantages described in ref. Roberts et al., 2018). Hence, we employ a state-of-the-art, ultra-high-resolution, fully coupled climate model, the Community Earth System Model, version 1.2.2 (referred as CESM-UHR, see ref. (Chu et al., 2020) for more details about CESM-UHR experiments and observed biases). The atmospheric component is the Community Atmosphere Model, version 5 (CAM5(Neale et al., 2012)), with a horizontal resolution of about 25 km and 30 vertical layers, allowing realistic regional details such as topography and local processes responsible for orographic processes(Sandu et al., 2019; Small et al., 2014; Tao et al., 2020). The sea surface temperature (SST) boundary conditions in CESM-UHR allows a more realistic representation of the ocean-atmosphere interactions and resolving of mesoscale oceanic features. We conducted a 140-year present-day (PD) simulation using an atmospheric CO_2 concentration of 367 ppm, initialized from a quasi-equilibrated climate state (Small et al., 2014). Two sensitivity experiments were carried out with CO_2 doubling (2×CO_2, 734 ppm) and CO_2 quadrupling (4×CO_2, 1468 ppm) (Chu et al., 2020). Other greenhouse gases have been kept at PD levels in each simulation. Each experiment was branched from the 71st year of the PD experiment and further integrated for 100 model years with prescribed CO_2 concentrations. To investigate the role of greenhouse warming on hydroclimate over mountains, we analyzed the equilibrated last 20 years of each simulation.

3 Methods

Classifying the mountains

Mountains can be classified based on topographic elevation and surface roughness. This study considered a topographic elevation of more than 1 km as a mountain. However, due to the limited horizontal resolution of the model, we were unable to include mountains with a terrain aspect of less than 25 km in our study (e.g., Western Ghats in India, Mt. Kilimanjaro in East Africa, and Highlands in Myanmar).

Vertically integrated moisture flux (kg m^{-1} day^{-1})

The vertically integrated moisture flux (Q) is the horizontal transport of atmospheric moisture by the penetrating winds, as:

$$Q = \frac{1}{g}\int_{1000hPa}^{100hPa} qV\,\partial p$$

where V is horizontal wind velocity, q is specific humidity, g is gravitational constant, and p is the atmospheric pressure.

Vertical cross-sections

Here, we studied the vertical structure to understand the associated processes rather than taking the vertical column average. Either latitude or longitude was chosen for cross-sections in detail based on the change in precipitation and associated vertically integrated moisture advection over the mountain.

Local saturated condensation (g kg^{-1} day^{-1})

Considering that environmental thermodynamics generally follows a moist adiabat, the local saturated condensation rate(Smith, 1979) caused by the adiabatic lifting can be approximated by:

$$c = -\left(\omega_a . \frac{\partial q_s}{\partial p}\right)$$

where ω_a is the ascending vertical velocity, and q_s is the saturated specific humidity.

Saturated specific humidity (**g kg^{-1}**)

Here, we define saturated specific humidity using an empirical method, where saturation vapor pressure (e*) is calculated using the Tetens equation(Murray, 1967).

$$q_s = 0.622\left(\frac{e^*}{p}\right)$$

Static stability (K hPa^{-1})

Static stability is stability of the atmosphere from hydrostatic equilibrium to vertical displacements. We investigated simple static stability using the following equation:

$$s = -\left(\frac{T}{\theta}\right)\left(\frac{\partial \theta}{\partial p}\right)$$

where T is the absolute air temperature and θ is the potential temperature.

Total diabatic heating (K day^{-1})

To understand the heating source in the atmosphere, the total diabatic heating rate(Nigam et al., 2000; Wang et al., 2019) is calculated using the potential temperature, which has conservation properties like those of dry static energy, approximated as:

$$Q_{diabatic} = \frac{T}{\theta}\left(\frac{\partial \theta}{\partial t} + \omega \frac{\partial \theta}{\partial p} + V_h . \nabla\theta\right)$$

where ω is the vertical velocity.

Moist static energy (kJ kg^{-1})

The moist static energy (h) is used as a thermodynamic variable, which represents the addition of dry static energy (DSE, sum of dry air enthalpy and potential energy) and latent static energy (LSE, latent atmospheric heat), as:

$$h = \left(C_p T + gz\right) + (L_v q)$$

where C_p is specific heat at constant pressure, z is the height above the surface, and L_v is the latent heat of vaporization.

Moisture budget analysis (mm day^{-1})

The vertically integrated moisture budget can be expressed as a linearized equation in terms of precipitation P, where E is evaporation, V is vertical moisture advection and H is horizontal moisture advection. We can neglect the moisture tendency term on the annual time scale, as it's small compared to the rest of terms in the moisture budget (Oueslati et al., 2019):

$$P = E + V + H$$

$$= E - \langle \omega . \frac{\partial q}{\partial p} \rangle - \langle V_h . \nabla q \rangle$$

Consequently, the change in mean precipitation can be expressed as follow:

$$\Delta P = \Delta E + \Delta V + \Delta H$$

Here angle brackets indicate a vertical mass integral, and delta indicates the change in mean state response to CO_2 perturbation of the respective quantity.

Vertical decomposition of moist static energy advection (kJ kg^{-1} day^{-1})

Atmospheric deep convection is mainly constrained by the moist static energy budget(Neelin & Held, 1987) and can be explained using the vertical structure of moist static energy advection. We decomposed vertical moist static energy advection into its dynamic and thermodynamic components.

$$-\Delta \left(\omega . \frac{\partial h}{\partial p} \right) = -\left(\Delta\omega . \frac{\partial \overline{h}}{\partial p} \right) - \left(\overline{\omega} . \frac{\partial \Delta h}{\partial p} \right)$$

$$= dynamic + Therodynamic$$

Quantifying the precipitation extremes

We used the following indices(Karl et al., 1999) to identify projected changes in extreme rainfall events.

The *simple daily intensity index (SDII, mm day*$^{-1}$*)* describes the daily precipitation amount averaged over all wet days in a year. The wet days are when precipitation exceeds more or equals 1 mm day^{-1}. *SDII* is an absolute index used to assess the intensity of extreme precipitation.

The *extreme flooding index (Rx5day, mm)* describes the maximum precipitation amount in five consecutive days. *Rx5day* is generally used to express the changes in likely flood risks, as heavy rain conditions can contribute to flooding conditions over consecutive days.

4 Results and Discussion

Projected elevation-dependent precipitation changes

Generally, the location of the mountain precipitation is determined by local factors (Boos & Pascale, 2021; Smith, 1979, 2018) such as mountain geometry, terrain steepness, surface wind, moisture source, etc. Considering the solidity of mountain geometry, which will not change in the future, changes in surface temperature due to global warming may lead to changes in other factors, such as surface wind and moisture sources. We examine the response of annual mean precipitation to surface local warming (Fig. 1). A global picture of projected temperature changes reveals that mountain systems are susceptible to greenhouse warming (Fig. S1). The response of annual mean precipitation seems more dominant over low-latitudinal mountains (30°S-30°N) as compared to the mountains in high-latitude in the 4×CO_2 experiment (Fig. 1). Strong response in these low-latitude regions can also be linked to the more substantial enhancement of water vapor in the low-latitude than high-latitude and changes in large-scale circulation patterns such as ITCZ(Mamalakis et al., 2021), MJO (Maloney et al., 2019; Roxy et al., 2019), and ENSO (Latif & Keenlyside, 2009; Mamalakis et al., 2021) under greenhouse warming. However, this study emphasizes the regional scale process only because precipitation response is very high over limited areas, implying that changes in regional climate are the dominant factor in the context of mountain precipitation changes. This analysis identifies five mountain regions experiencing significant precipitation changes in response to CO_2 quadrupling. Based on the area that exceeds precipitation response to the local warming by a threshold $\pm$ 0.1 mm/day/°C, we selected the five most prominent regions among the global mountain range: New Guinea, East Africa, Eastern Himalaya, Central America, and Central Andes (Fig. 1a-e). Since the high-resolution simulation can decently capture topographic features, the mean precipitation pattern in the CESM-UHR simulation over mountain ranges seems reliable compared to the CESM-CMIP6 (100 km nominal resolution) (see Fig. S2). The reliability and accuracy of CMIP6 models are restricted due to their utilization of a coarser resolution. However, precipitation biases in CESM-UHR simulation over some regions analogized to satellite observations are very likely due to the model configuration.

The notable changes in precipitation are most likely at high elevations (Fig. S3a-e) under CO_2-induced warming but still are highly uncertain (Hock et al., 2019). Based on the precipitation change over five mountain regions, we define wetting mountains (New Guinea, East Africa, Eastern Himalayas, windward side of Central Andes) where the precipitation increases and drying mountains (Central America, the leeward side of Central Andes) where the precipitation decreases in a CO_2-enriched climate. Interestingly, the spatial pattern of anomalous precipitation over an individual mountain is heterogeneous, predominantly evident at mount summits or steep terrain (Fig. 1), and looks like elevation-dependent precipitation change. The most increase in precipitation intensity is exhibited at Puncak Jaya in New Guinea (Fig. 1a and Fig. S3a). In contrast, there is an overall drying over Central America (Fig. 1d). It should be noted that the highest mountain summit (e.g., Himalayan peaks) experiences inadequate precipitation due to a lack of moisture supply. In such cases (like Eastern Himalaya, Fig. 1c and Fig. S3c), it precipitates over steep topography before reaching the high summit. Central Andes exhibits both responses, wetting over the windward side of Central Andes and drying over the leeward side of Central Andes.

Atmospheric conditions

The moisture advection over the mountains strongly depends on its terrain pattern, which plays an important role in shaping the vertical profile of moisture content and regional atmospheric conditions. The atmospheric relative humidity is assumed to have increased (Tamarin-Brodsky & Hadas, 2019) under a warming scenario through an oceanic pathway, where the Clausius–Clapeyron relation governs the increase in saturation-specific humidity (O'Gorman & Muller, 2010). It is observed that the change in precipitation (Fig. 1) is linked to the vertical structure of the relative humidity (Fig. 2k-o). The major contributor to the precipitation changes is mostly upslope lifting over the mountain terrain (Smith, 1979, 2018; Tao et al., 2020), which change can influence atmospheric humidity and surface wind. The enhancement and reduction of vertical motion are more evident on the mountain summit and slope (Fig. 3). These enhancements are consistently replicated in the 2×CO_2 and 4×CO_2 experiments. Also, updrafts are widespread in the upper level over projected wet (Fig. 2k, l, m, o) and downdrafts over projected drying (Fig. 2n and o) mountains. These results show that moisture influences the vertical motion over mountainous terrain in the projected CO_2-induced warming scenario. The projected precipitation changes in mountain regions are described in terms of the changes in local saturated condensation (Fig. 3), which is a function of saturated humidity and upward vertical velocity. The diabatic heating influences atmospheric stability (black contour in Fig. 4) at the upper level. Fig. 4 highlights the atmospheric stabilization condition. Atmospheric stabilization refers to the resistance of the atmosphere to vertical motion, which can inhibit the development of deep convection, as it makes it harder for air to rise and form deep convection.

Changes in vertical velocity agree well with strengthening moist static energy through latent heat release. A unique core of least moist static energetics can be observed in the vicinity of mountain summits (Fig. 5a-e) in PD climate, which is strengthened in both 2×CO_2 (Fig. 5f-j) and 4×CO_2 experiments (Fig. 5k-o). The atmospheric moist static energy is enhanced overall in a projected CO_2-induced greenhouse warming scenario, followed by lower-level latent static energy. Additionally, precipitation causes additional local moistening and subsequently enhances the latent static energy with a vertical extension of moist static energy (Fig. 5). In drying mountain regions, raised lower-level dry static energy (Fig. 5n, o) can be seen where restricted diabatic surface heating and upper-level cooling (Fig. 4n, o). In addition, we marked an anomalous dry static environment under CO_2 perturbation in these unfavorable regions for upward motion.

Role of moist dynamics

Moisture budget analysis (see Methods and Fig. 6) shows vertical moisture advection has a close relationship with precipitation in the PD and CO_2 experiments (this close relationship can only be found over the wetter area), consistent with previous studies (Oueslati et al., 2019; Yang et al., 2014). Sufficient moisture in the atmospheric column and strong vertical motions resulted in wetting over mountain regions. This framework has been generally utilized to compare local changes in precipitation (Bony et al., 2013; Chou et al., 2012; Huang et al., 2013; Oueslati et al., 2019; Wang et al., 2019). Wetting mountains consistently increase precipitation and vertical moisture advection, whereas drying mountains do not. However, horizontal moisture advection is small compared to vertical moisture advection (Fig. 7). An anomalous increase in moisture advection can be found in the atmosphere over mountains, consistent with precipitation increase, whereas an anomalous decrease in moisture advection with precipitation decrease (Fig. 6 and 7). The moisture advection response (see Supplementary Methods and Fig. S5) is analyzed using vertical moisture advection (in terms of dynamic and thermodynamic components) and horizontal moisture advection. Our results suggest that vertical advection leads to more moisture (Fig. 7), which causes more latent heating, strengthening the upward motion through the thermodynamic factors (Fig. S5) at lower-level closer to the steep mountain terrain. For example, Eastern Himalayas have the thermodynamic component triggered at a lower level from foothills to steep terrain, further reshaping the upper-level dynamic contribution (see Fig. S4h and c). Even though horizontal advection has slight changes over most of the mountains, it plays a crucial role in the windward side of the Central Andes (peripheral to the Pacific Ocean; Fig. 7o and S4o). Using the moist advection approach to understand the seasonal cycle (Fig. 7) and its complexity to explain the observed pattern seems complicated. We endeavored to improve our understanding of the intricate patterns observed in both Central America and the Central Andes using deep convection. Our objective was to gain insights into the multiple factors contributing to the complex patterns observed, including moisture distribution and atmospheric circulation. To achieve this, we studied the role of deep convection and its impact on these patterns.

Atmospheric deep convection

Atmospheric deep convection occurs in the tropics and is mainly associated with vertical motion, causing diabatic heating and moist static energy export (Bui et al., 2016; Neelin & Held, 1987; Yan et al., 2020). Also, as vertical moisture advection plays a dominant role in mountain hydroclimate response to CO_2 quadrupling, we split vertical moist static energy advection into dynamic and thermodynamic components (see Methods). Positive (negative) vertical MSE advection involves the transport of higher (lower) energy in the vertical direction, resulting in an increase (decrease) of available energy in the atmosphere. This can help us explain the respective contribution of energy import or export and its possible linkage to vertical motion. A symmetric pattern (Fig. 8) is observed over mountains with a low-level energy import. Interestingly, this symmetric pattern of moist energetic response shows consistent results with precipitation changes.

In wet regions such as East Africa, the Eastern Himalayas, Central America, and the windward side of Central Andes, there is a positive thermodynamic component in the lower atmosphere (Fig. 8i, m, o) and a negative dynamic component at the upper level (Fig. 8g, h, e). In New Guinea, both thermodynamic and dynamic responses are similar in the lower atmosphere (Fig. 8f and k), which leads to enhanced deep convection and intense precipitation. However, drying mountains have energy imports at lower and upper levels (Fig. 8d, e). At the upper level in Central America and the leeward side of Central Andes, positive dynamic responses (as shown in Fig. 8i and j) impede convection and reduce precipitation. We demonstrated that warming in mountainous areas amplifies the thermodynamic effect (Moustakis et al., 2020) in the lower atmosphere. Based on our analysis, we can infer that the cause of deep convection in wet regions is attributed to the increase in thermodynamic components at a low level and the decrease in dynamic components at the upper level. However, shallow-hinder convection is observed in dry regions due to the increase in the thermodynamic component at a low level and the dynamic component at an upper level.

Orographic moist-convection feedback

An increase in static stability is unfavorable for vertical motion as more upper-level warming will create a more stable troposphere. Several studies (Li & O'Gorman, 2020; Maloney et al., 2019; Sharmila & Walsh, 2018; Shi & Durran, 2015) have shown that global warming leads to increased atmospheric stability, which in turn can cause the atmosphere to become more stratified. Hypothetically, the mountains are supposed to be wetter under a warming scenario, as they can accumulate additional moisture content owing to temperature rise. Similar to conclusions from previous studies (see refs. Li and O'Gorman, 2020; Shi and Durran, 2016, 2015, 2014; Zhao et al., 2020) on the midlatitude mountains, raising moisture in vertical ascending motion results in anomalous diabatic heating through enhanced condensation and triggers precipitation extremes. This anomalous heating is thermodynamically compensated with ascending vertical motion, which sucks moisture from the lower atmosphere (Lau et al., 2020; Tamarin-Brodsky & Hadas, 2019). What determines the precipitation changes over mountains under the future warming climate? We attempted to answer this question by using feedback mechanisms. Herein, we introduce the concept of "Orographic moist-convection" feedback, explaining the loop mechanism in which vertical motion is reshaped by moisture over a mountain in a warming climate that can further amplify or dampen through feedback and vice versa (schematically illustrated in Fig. 9). In response to CO_2 forcing, the wetting mountain regions are found to be associated with wetting response. Wind speed should reduce due to the weaker zonal temperature gradient in warm tropical climates but more moisture gradient (Maloney et al., 2019; Sohn et al., 2019; Vecchi & Soden, 2007). Therefore, a more humid hydroclimate mountain drops the lifted condensation levels. This abundant moisture content elongates the ascending motion by diabatic heating. Precipitation increases are attributed to the wetting response, further amplified by enhanced ascending motion under CO_2 perturbation (Fig. 9a). A substantial increase in diabatic heating leads to deeper vertical heating at upper levels of the atmosphere, supporting deep convection with vertically rising moist static energy from a low level is also favorable for ascending motion. But it coexists with an overall increase in atmospheric stability in the background, which shows this increase in stability would increase the lapse rate (Fig. S3u-y). Deep moist convection in the mountains can counteract the regional lapse rate within this framework. We confirm that the resultant moist-convection feedback appears positive after compensating with processes. On the other hand, the drying mountains are manifested by the drying response of orographic moist-convection feedback (Fig. 9b). The drying regions experience a decrease in saturated moisture content, which leads to a reduction in upward air movement. This is caused by a diabatic cooling anomaly at a lower level, resulting in shallow convection. As a result, the initial humidity is further decreased. Atmospheric stabilization is a counterpart in both responses to maintain equilibrium within the feedback loop. Low-level relative humidity response shows why the initial trigger in some mountainous areas differs from others, as the response increased nearby wetting mountains and decreased nearby drying mountains (Fig. S6). These results indicate that the orographic moist-convection feedback that modifies regional precipitation is evident. Differences in the strength of the feedback on a regional scale can result in varying precipitation responses.

Extreme event reverberation

Extreme events are strongly associated with a change in the mean climate state. Regional atmospheric conditions and local topography strongly affect these extreme events (Zhang & Liang, 2020). Geographical features concerning topography significantly modulate the spatial changes in extreme events (Herold et al., 2016; Shi & Durran, 2015). Besides, change in the background temperature due to CO_2-induced greenhouse warming also contributes to the variability of extreme precipitation. To further understand the change in extreme events in response to CO_2 quadrupling, we examine extremes (Karl et al., 1999) using absolute precipitation criteria (see Methods and Fig. 10), such as the precipitation intensity (SDII) and extreme flooding events (Rx5day). These events (Fig. 10a-e and Fig. S5a-e) coincide with their mean precipitation changes (Fig. 1a-e and Fig. S5a-e) under CO_2-induced greenhouse gas forcing, increasing the events over New Guinea, East Africa, Eastern Himalaya, mountains part of Central Andes, and decreasing over Central America and leeward side of Central Andes. However, certain extreme events are not related to changes in precipitation mean states, like the highest precipitation in 1-day and 5-day over the Eastern Himalayan region (Fig. S5h and m) and heavy rainy days over the Central Andes (Fig. S5t). These amplified events exceed precipitation anomalies, which further exclusively need to be investigated. Time-dependent indices like heavy rainy days R10, R20 (Fig. S5p-t and S5u-y) concurrently pick through vertical moisture advection (consistent with previous attributional studies (O'Gorman et al., 2021; Oueslati et al., 2019; Zhao et al., 2020)). The consequences of such excessive extremes are responsible for excessive surface runoff (Fig. S3k-o), further exacerbating hazards such as river floods, mountain landslides, and debris flow in the mountains and their surrounding regions (Moustakis et al., 2020). It is possible that the CESM-UHR model may have limitations when simulating extreme precipitation in mountainous regions, as these events are often influenced by complex and localized processes that can be challenging to represent accurately in models.

5 Conclusions

The CESM-UHR provides a valuable opportunity for studying regional climate change in a specific region. In the present study, we employed CESM-UHR to address future changes in precipitation patterns in mountain regions due to increasing CO_2 concentrations in the earth's atmosphere. The five most sensitive mountains in the low latitude, including New Guinea, East Africa, Eastern Himalayas, Central America, and Central Andes, are identified based on precipitation response. A comprehensive feedback framework describes the change in precipitation response to adjustments in the mean state of vertical structure and its related processes. Our study proposes "Orographic moist-convection feedback" for precipitation attributions which appear as positive feedback in the climate system, amplifying an initial state. This feedback consists of two primary net responses, wet and drying responses. In the case of wetting response, the warming-induced moisture addition in the mountain terrain favors a strengthening of ascending motion and anomalous diabatic heating through enhanced precipitation, which further enhances the local build-up of humidity. But, in the case of drying response, the moisture shortage restricts the ascending motion, reducing local precipitation and further reducing the moisture. Orographic moist-convection feedback response to CO_2 perturbations could explain the projected wetting in New Guinea, East Africa, the Eastern Himalayas, the windward side of Central Andes, and projected drying in Central America and the leeward side of Central Andes.

Even though our study concentrates on the mean state changes, the proposed feedback mechanism can potentially improve our comprehension of future changes in mountain precipitation variability from diurnal to interannual timescales. The precipitation changes over the mountains can cause other significant threats, such as mountain-ice melting (Chen et al., 2013), loss and degradation of soil (Borrelli et al., 2020), and biodiversity reduction (Peters et al., 2019; Viviroli et al., 2007), which pose severe consequences to humans and the entire our ecosystem (Conway et al., 2019; Elsen et al., 2020). Thus, climate change-induced regional hydroclimatic changes pose formidable challenges to decision-makers in ensuring mountain water management and resilience. The scientific community can apply this framework to investigate the potential threats to water resource management and related biodiversity. Policymakers need to adopt strategic planning risk mitigation related to the mountains and regions highly dependent on mountain resources.

Acknowledgments

The authors wish to acknowledge the use of the PyFerret program for analysis and graphics in this paper. PyFerret is a product of NOAA's Pacific Marine Environmental Laboratory (Information is available at https://ferret.pmel.noaa.gov/Ferret/). The Earth system model used in our study is the Community Earth System Model version 1.2.2 (CESM1.2.2) developed at the National Center for Atmospheric Research. The source code for CESM releases is distributed through a public subversion code repository, CESM1.2 release page is https://www2.cesm.ucar.edu/models/cesm1.2/. The simulations were conducted on the IBS/ICCP supercomputer "Aleph" 1.43 petaflops high-performance Cray XC50-LC Skylake computing system with 18,720 processor cores, 9.59 petabytes storage, and 43 petabytes tape archive space. With heartfelt appreciation, PK acknowledges Axel Timmermann for their invaluable contributions during the initial discussion, which played a crucial role in shaping the content of this work. Authors to extend sincere appreciation to Jahfer Sharif for proofreading and suggestions.

Funding

PK was supported by the National Research Foundation of Korea (NRF) grant funded by the Korean government (MSIT) (Grant No. 2020R1A2C2006860). KH and SL were supported by the Institute for Basic Science (IBS-R028-D1).

Open Research

All data used in this study are publicly available.

The CESM1.2.2 model simulation data are available at https://ibsclimate.org/research/ultra-high-resolution-climate-simulation-project.

The satellite 3B43 dataset was obtained from the Tropical Rainfall Measurement Mission (TRMM, http://doi.org/10.5067/TRMM/TMPA/MONTH/7).

CESM2 model simulation data available at Coupled Model Intercomparison Project Phase 6 (CMIP6) provided by ESGF link (https://esgf-node.llnl.gov/projects/cmip6/). Users should select the source id as CESM2.

Author Contributions

PK and KH conceived the study and wrote the initial manuscript draft. PK performed the analysis and investigation and prepared all the figures. SL conducted the model simulations. JC assisted in model data extraction. All authors interpreted the results and contributed to improving the final manuscript.

References

Bony, S., Bellon, G., Klocke, D., Sherwood, S., Fermepin, S., & Denvil, S. (2013). Robust direct effect of carbon dioxide on tropical circulation and regional precipitation. *Nature Geoscience*, *6*(6). https://doi.org/10.1038/ngeo1799

Boos, W. R., & Pascale, S. (2021). Mechanical forcing of the North American monsoon by orography. *Nature*, *599*(7886), 611–615. https://doi.org/10.1038/s41586-021-03978-2

Borrelli, P., Robinson, D. A., Panagos, P., Lugato, E., Yang, J. E., Alewell, C., et al. (2020). Land use and climate change impacts on global soil erosion by water (2015-2070). *Proceedings of the National Academy of Sciences of the United States of America*, *117*(36). https://doi.org/10.1073/pnas.2001403117

Bui, H. X., Yu, J. Y., & Chou, C. (2016). Impacts of vertical structure of large-scale vertical motion in tropical climate: Moist static energy framework. *Journal of the Atmospheric Sciences*, *73*(11). https://doi.org/10.1175/JAS-D-16-0031.1

Chen, J. L., Wilson, C. R., & Tapley, B. D. (2013). Contribution of ice sheet and mountain glacier melt to recent sea level rise. *Nature Geoscience*, *6*(7). https://doi.org/10.1038/ngeo1829

Chou, C., Chen, C. A., Tan, P. H., & Chen, K. T. (2012). Mechanisms for global warming impacts on precipitation frequency and intensity. *Journal of Climate*, *25*(9), 3291–3306. https://doi.org/10.1175/JCLI-D-11-00239.1

Chu, J.-E., Lee, S.-S., Timmermann, A., Wengel, C., Stuecker, M. F., & Yamaguchi, R. (2020). Reduced tropical cyclone densities and ocean effects due to anthropogenic greenhouse warming. *Science Advances*, *6*(51), eabd5109. https://doi.org/10.1126/sciadv.abd5109

Colle, B. A., Smith, R. B., & Wesley, D. A. (2013). Theory, Observations, and Predictions of Orographic Precipitation. https://doi.org/10.1007/978-94-007-4098-3_6

Conway, D., Nicholls, R. J., Brown, S., Tebboth, M. G. L., Adger, W. N., Ahmad, B., et al. (2019). The need for bottom-up assessments of climate risks and adaptation in climate-sensitive regions. *Nature Climate Change*, *9*(7). https://doi.org/10.1038/s41558-019-0502-0

Elsen, P. R., Monahan, W. B., & Merenlender, A. M. (2020). Topography and human pressure in mountain ranges alter expected species responses to climate change. *Nature Communications*, *11*(1). https://doi.org/10.1038/s41467-020-15881-x

Grose, M. R., Syktus, J., Thatcher, M., Evans, J. P., Ji, F., Rafter, T., & Remenyi, T. (2019). The role of topography on projected rainfall change in mid-latitude mountain regions. *Climate Dynamics*, *53*(5–6). https://doi.org/10.1007/s00382-019-04736-x

Gutowski, W. J., Ullrich, P. A., Hall, A., Leung, L. R., O'Brien, T. A., Patricola, C. M., et al. (2021). The ongoing need for high-resolution regional climate models: Process understanding and stakeholder information. *Bulletin of the American Meteorological Society*, *101*(5). https://doi.org/10.1175/BAMS-D-19-0113.1

Herold, N., Alexander, L. v., Donat, M. G., Contractor, S., & Becker, A. (2016). How much does it rain over land? *Geophysical Research Letters*, *43*(1). https://doi.org/10.1002/2015GL066615

Hock, R., Rasul, G., Adler, C., Cáceres, B., Gruber, S., Hirabayashi, Y., et al. (2019). Chapter 2: High Mountain Areas. IPCC Special Report on the Ocean and Cryosphere in a Changing Climate. In *IPCC Special Report on the Ocean and Cryosphere in a Changing Climate*.

Huang, P., Xie, S. P., Hu, K., Huang, G., & Huang, R. (2013). Patterns of the seasonal response of tropical rainfall to global warming. *Nature Geoscience*, *6*(5). https://doi.org/10.1038/ngeo1792

Huss, M., Bookhagen, B., Huggel, C., Jacobsen, D., Bradley, R. S., Clague, J. J., et al. (2017). Toward mountains without permanent snow and ice. *Earth's Future*, *5*(5), 418–435. https://doi.org/10.1002/2016EF000514

Immerzeel, W. W., Lutz, A. F., Andrade, M., Bahl, A., Biemans, H., Bolch, T., et al. (2020). Importance and vulnerability of the world's water towers. *Nature*, *577*(7790), 364–369. https://doi.org/10.1038/s41586-019-1822-y

Kad, P., Blau, M. T., Ha, K.-J., & Zhu, J. (2022). Elevation-dependent temperature response in early Eocene using paleoclimate model experiment. *Environmental Research Letters*, *17*(11), 114038. https://doi.org/10.1088/1748-9326/ac9c74

Karl, T. R., Nicholls, N., & Ghazi, A. (1999). CLIVAR/GCOS/WMO Workshop on Indices and Indicators for Climate Extremes - Workshop summary. In *Climatic Change* (Vol. 42). https://doi.org/10.1023/A:1005491526870

Latif, M., & Keenlyside, N. S. (2009). El Niño/Southern Oscillation response to global warming. *Proceedings of the National Academy of Sciences of the United States of America*, *106*(49). https://doi.org/10.1073/pnas.0710860105

Lau, W. K. M., Kim, K. M., Chern, J. D., Tao, W. K., & Leung, L. R. (2020). Structural changes and variability of the ITCZ induced by radiation–cloud–convection–circulation interactions: inferences from the Goddard Multi-scale Modeling Framework (GMMF) experiments. *Climate Dynamics*, *54*(1–2). https://doi.org/10.1007/s00382-019-05000-y

Li, Z., & O'Gorman, P. A. (2020). Response of vertical velocities in extratropical precipitation extremes to climate change. *Journal of Climate*, *33*(16). https://doi.org/10.1175/JCLI-D-19-0766.1

Maloney, E. D., Adames, Á. F., & Bui, H. X. (2019). Madden–Julian oscillation changes under anthropogenic warming. *Nature Climate Change*. https://doi.org/10.1038/s41558-018-0331-6

Mamalakis, A., Randerson, J. T., Yu, J. Y., Pritchard, M. S., Magnusdottir, G., Smyth, P., et al. (2021). Zonally contrasting shifts of the tropical rain belt in response to climate change. *Nature Climate Change*, *11*(2). https://doi.org/10.1038/s41558-020-00963-x

Mountains of change. (2021). *Nature Geoscience*, *14*(2), 57–57. https://doi.org/10.1038/s41561-021-00694-4

Moustakis, Y., Onof, C. J., & Paschalis, A. (2020). Atmospheric convection, dynamics and topography shape the scaling pattern of hourly rainfall extremes with temperature globally. *Communications Earth & Environment*, *1*(1). https://doi.org/10.1038/s43247-020-0003-0

Murray, F. W. (1967). On the Computation of Saturation Vapor Pressure. *Journal of Applied Meteorology*, *6*(1). https://doi.org/10.1175/1520-0450(1967)006<0203:otcosv>2.0.co;2

Napoli, A., Crespi, A., Ragone, F., Maugeri, M., & Pasquero, C. (2019). Variability of orographic enhancement of precipitation in the Alpine region. *Scientific Reports*, *9*(1). https://doi.org/10.1038/s41598-019-49974-5

Neale, R. B., Gettelman, A., Park, S., Chen, C., Lauritzen, P. H., Williamson, D. L., et al. (2012). Description of the NCAR Community Atmosphere Model (CAM 5.0). NCAR Technical Notes. *Ncar/Tn-464+Str*.

Neelin, J. D., & Held, I. M. (1987). Modeling tropical convergence based on the moist static energy budget. *Monthly Weather Review*, *115*(1). https://doi.org/10.1175/1520-0493(1987)115<0003:MTCBOT>2.0.CO;2

Nigam, S., Chung, C., & DeWeaver, E. (2000). ENSO diabatic heating in ECMWF and NCEP-NCAR reanalyses, and NCAR CCM3 simulation. *Journal of Climate*, *13*(17). https://doi.org/10.1175/1520-0442(2000)013<3152:EDHIEA>2.0.CO;2

O'Gorman, P. A., & Muller, C. J. (2010). How closely do changes in surface and column water vapor follow Clausius-Clapeyron scaling in climate change simulations? *Environmental Research Letters*, *5*(2). https://doi.org/10.1088/1748-9326/5/2/025207

O'Gorman, P. A., Li, Z., Boos, W. R., & Yuval, J. (2021). Response of extreme precipitation to uniform surface warming in quasi-global aquaplanet simulations at high resolution. *Philosophical Transactions of the Royal Society A: Mathematical, Physical and Engineering Sciences*, *379*(2195). https://doi.org/10.1098/rsta.2019.0543

Oueslati, B., Yiou, P., & Jézéquel, A. (2019). Revisiting the dynamic and thermodynamic processes driving the record-breaking January 2014 precipitation in the southern UK. *Scientific Reports*, *9*(1). https://doi.org/10.1038/s41598-019-39306-y

Pepin, N., Bradley, R. S., Diaz, H. F., Baraer, M., Caceres, E. B., Forsythe, N., et al. (2015). Elevation-dependent warming in mountain regions of the world. *Nature Climate Change*. https://doi.org/10.1038/nclimate2563

Pepin, N. C., Arnone, E., Gobiet, A., Haslinger, K., Kotlarski, S., Notarnicola, C., et al. (2022). Climate Changes and Their Elevational Patterns in the Mountains of the World. *Reviews of Geophysics*, *60*(1). https://doi.org/10.1029/2020rg000730

Peters, M. K., Hemp, A., Appelhans, T., Becker, J. N., Behler, C., Classen, A., et al. (2019). Climate–land-use interactions shape tropical mountain biodiversity and ecosystem functions. *Nature*, *568*(7750). https://doi.org/10.1038/s41586-019-1048-z

Rangwala, I., & Miller, J. R. (2012). Climate change in mountains: A review of elevation-dependent warming and its possible causes. *Climatic Change*, *114*(3–4). https://doi.org/10.1007/s10584-012-0419-3

Roberts, M. J., Vidale, P. L., Senior, C., Hewitt, H. T., Bates, C., Berthou, S., et al. (2018). The benefits of global high resolution for climate simulation process understanding and the enabling of stakeholder decisions at the regional scale. *Bulletin of the American Meteorological Society*, *99*(11). https://doi.org/10.1175/BAMS-D-15-00320.1

Roe, G. H., & Baker, M. B. (2006). Microphysical and geometrical controls on the pattern of orographic precipitation. *Journal of the Atmospheric Sciences*, *63*(3). https://doi.org/10.1175/JAS3619.1

Roxy, M. K., Dasgupta, P., McPhaden, M. J., Suematsu, T., Zhang, C., & Kim, D. (2019). Twofold expansion of the Indo-Pacific warm pool warps the MJO life cycle. *Nature*, *575*(7784). https://doi.org/10.1038/s41586-019-1764-4

Sandu, I., van Niekerk, A., Shepherd, T. G., Vosper, S. B., Zadra, A., Bacmeister, J., et al. (2019). Impacts of orography on large-scale atmospheric circulation. *Npj Climate and Atmospheric Science*, *2*(1). https://doi.org/10.1038/s41612-019-0065-9

Sharmila, S., & Walsh, K. J. E. (2018). Recent poleward shift of tropical cyclone formation linked to Hadley cell expansion. *Nature Climate Change*, *8*(8). https://doi.org/10.1038/s41558-018-0227-5

Shi, X., & Durran, D. (2016). Sensitivities of extreme precipitation to global warming are lower over mountains than over oceans and plains. *Journal of Climate*, *29*(13). https://doi.org/10.1175/JCLI-D-15-0576.1

Shi, X., & Durran, D. R. (2014). The response of orographic precipitation over idealized midlatitude mountains due to global increases in CO2. *Journal of Climate*, *27*(11). https://doi.org/10.1175/JCLI-D-13-00460.1

Shi, X., & Durran, D. R. (2015). Estimating the response of extreme precipitation over midlatitude mountains to global warming. *Journal of Climate*, *28*(10). https://doi.org/10.1175/JCLI-D-14-00750.1

Siler, N., & Roe, G. (2014). How will orographic precipitation respond to surface warming? An idealized thermodynamic perspective. *Geophysical Research Letters*, *41*(7). https://doi.org/10.1002/2013GL059095

Siler, N., Roe, G., & Durran, D. (2013). On the dynamical causes of variability in the rain-shadow effect: A case study of the Washington Cascades. *Journal of Hydrometeorology*, *14*(1). https://doi.org/10.1175/JHM-D-12-045.1

Small, R. J., Bacmeister, J., Bailey, D., Baker, A., Bishop, S., Bryan, F., et al. (2014). A new synoptic scale resolving global climate simulation using the Community Earth System Model. *Journal of Advances in Modeling Earth Systems*, *6*(4). https://doi.org/10.1002/2014MS000363

Smith, R. B. (1979). The influence of mountains on the atmosphere. *Advances in Geophysics*, *21*(C). https://doi.org/10.1016/S0065-2687(08)60262-9

Smith, R. B. (2018). 100 years of progress on mountain meteorology research. *Meteorological Monographs*, *59*. https://doi.org/10.1175/AMSMONOGRAPHS-D-18-0022.1

Sohn, B. J., Yeh, S. W., Lee, A., & Lau, W. K. M. (2019). Regulation of atmospheric circulation controlling the tropical Pacific precipitation change in response to CO 2 increases. *Nature Communications*, *10*(1). https://doi.org/10.1038/s41467-019-08913-8

Sun, Q., Miao, C., Duan, Q., Ashouri, H., Sorooshian, S., & Hsu, K. L. (2018). A Review of Global Precipitation Data Sets: Data Sources, Estimation, and Intercomparisons. *Reviews of Geophysics*, *56*(1). https://doi.org/10.1002/2017RG000574

Tamarin-Brodsky, T., & Hadas, O. (2019). The Asymmetry of Vertical Velocity in Current and Future Climate. *Geophysical Research Letters*, *46*(1). https://doi.org/10.1029/2018GL080363

Tao, W., Huang, G., Lau, W. K. M., Dong, D., Wang, P., & Wen, G. (2020). How can CMIP5 AGCMs' resolution influence precipitation in mountain areas: the Hengduan Mountains? *Climate Dynamics*, *54*(1–2). https://doi.org/10.1007/s00382-019-04993-w

UN. United Nations Transforming Our World: the 2030 Agenda for Sustainable Development. A/RES/70/1, 16301 United Nations § (2015).

Vecchi, G. A., & Soden, B. J. (2007). Global warming and the weakening of the tropical circulation. *Journal of Climate*, *20*(17). https://doi.org/10.1175/JCLI4258.1

Viviroli, D., Dürr, H. H., Messerli, B., Meybeck, M., & Weingartner, R. (2007). Mountains of the world, water towers for humanity: Typology, mapping, and global significance. *Water Resources Research*, *43*(7). https://doi.org/https://doi.org/10.1029/2006WR005653

Wallace, J. M., & Hobbs, P. v. (2006). *Atmospheric Science: An Introductory Survey: Second Edition*. *Atmospheric Science: An Introductory Survey: Second Edition*. https://doi.org/10.1016/C2009-0-00034-8

Wang, M., Wang, J., Duan, A., Yang, J., & Liu, Y. (2019). Quasi-biweekly impact of the atmospheric heat source over the Tibetan Plateau on summer rainfall in Eastern China. *Climate Dynamics*, *53*(7–8). https://doi.org/10.1007/s00382-019-04798-x

Yan, Z., Wu, B., Li, T., Collins, M., Clark, R., Zhou, T., et al. (2020). Eastward shift and extension of ENSO-induced tropical precipitation anomalies under global warming. *Science Advances*, *6*(2). https://doi.org/10.1126/sciadv.aax4177

Yang, Q., Ruby Leung, L., Rauscher, S. A., Ringler, T. D., & Taylor, M. A. (2014). Atmospheric moisture budget and spatial resolution dependence of precipitation extremes in aquaplanet simulations. *Journal of Climate*, *27*(10). https://doi.org/10.1175/JCLI-D-13-00468.1

Zandler, H., Haag, I., & Samimi, C. (2019). Evaluation needs and temporal performance differences of gridded precipitation products in peripheral mountain regions. *Scientific Reports*, *9*(1). https://doi.org/10.1038/s41598-019-51666-z

Zemp, M., Huss, M., Thibert, E., Eckert, N., McNabb, R., Huber, J., et al. (2019). Global glacier mass changes and their contributions to sea-level rise from 1961 to 2016. *Nature*, *568*(7752). https://doi.org/10.1038/s41586-019-1071-0

Zhang, Y., & Liang, C. (2020). Analysis of Annual and Seasonal Precipitation Variation in the Qinba Mountain area, China. *Scientific Reports*, *10*(1). https://doi.org/10.1038/s41598-020-57743-y

Zhao, Y., Chen, D., Li, J., Chen, D., Chang, Y., Li, J., & Qin, R. (2020). Enhancement of the summer extreme precipitation over North China by interactions between moisture convergence and topographic settings. *Climate Dynamics*, *54*(5–6). https://doi.org/10.1007/s00382-020-05139-z

Figures

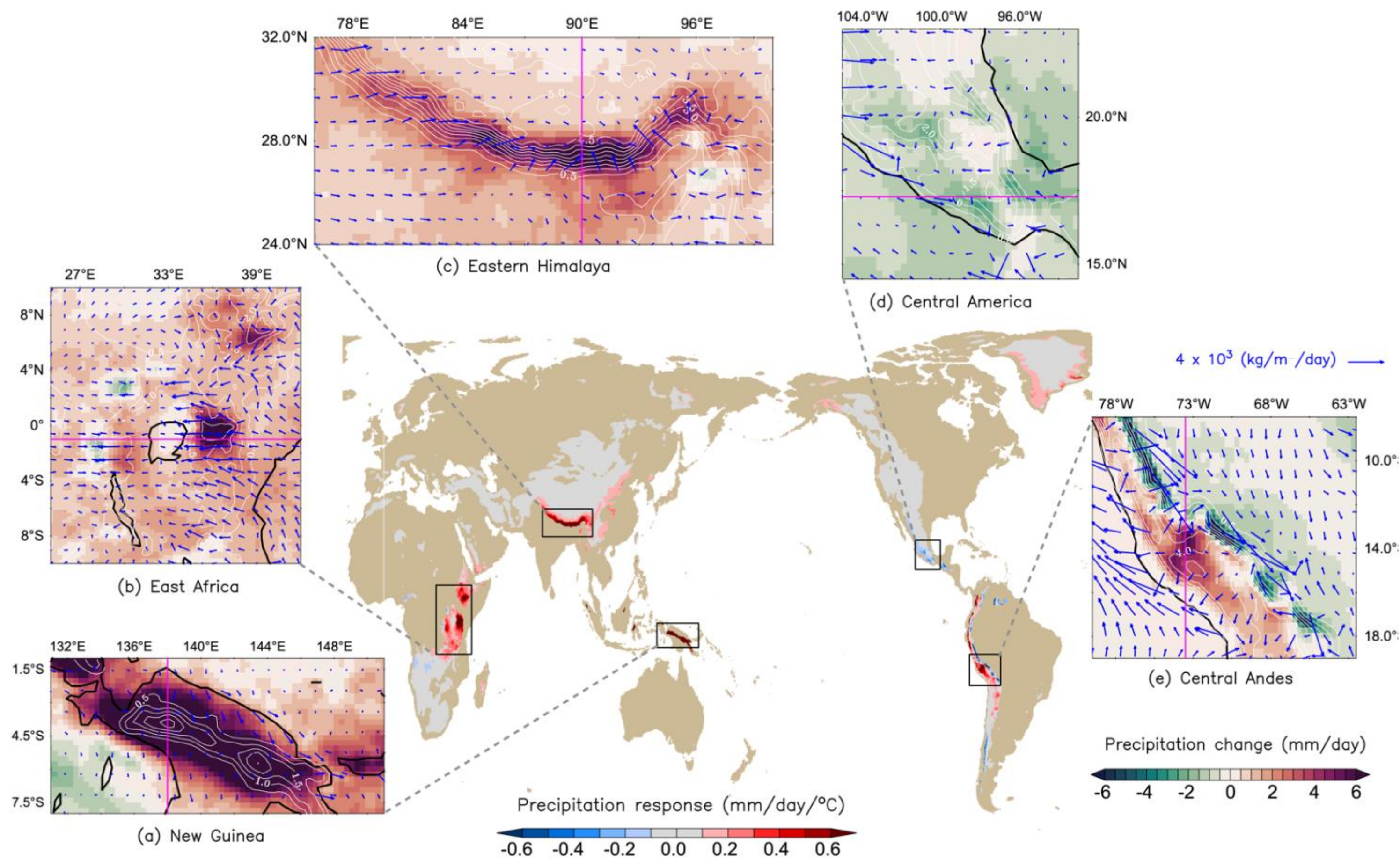

Fig. 1. Projected elevation-dependent precipitation changes over the global mountain in response to $4\times CO_2$. The center panel indicates precipitation response (absolute change in precipitation rate) to local warming associated with future change. The sub-panels indicate precipitation changes in $4\times CO_2$ compared to PD over (a) New Guinea, (b) East Africa, (c) Eastern Himalaya, (d) Central America, and (f) Central Andes. The blue vectors are vertically integrated horizontal moisture flux, and the white contour shows an elevation orography of 0.5 km interval. The magenta line indicates either the longitude or latitude of the cross-section for further analysis.

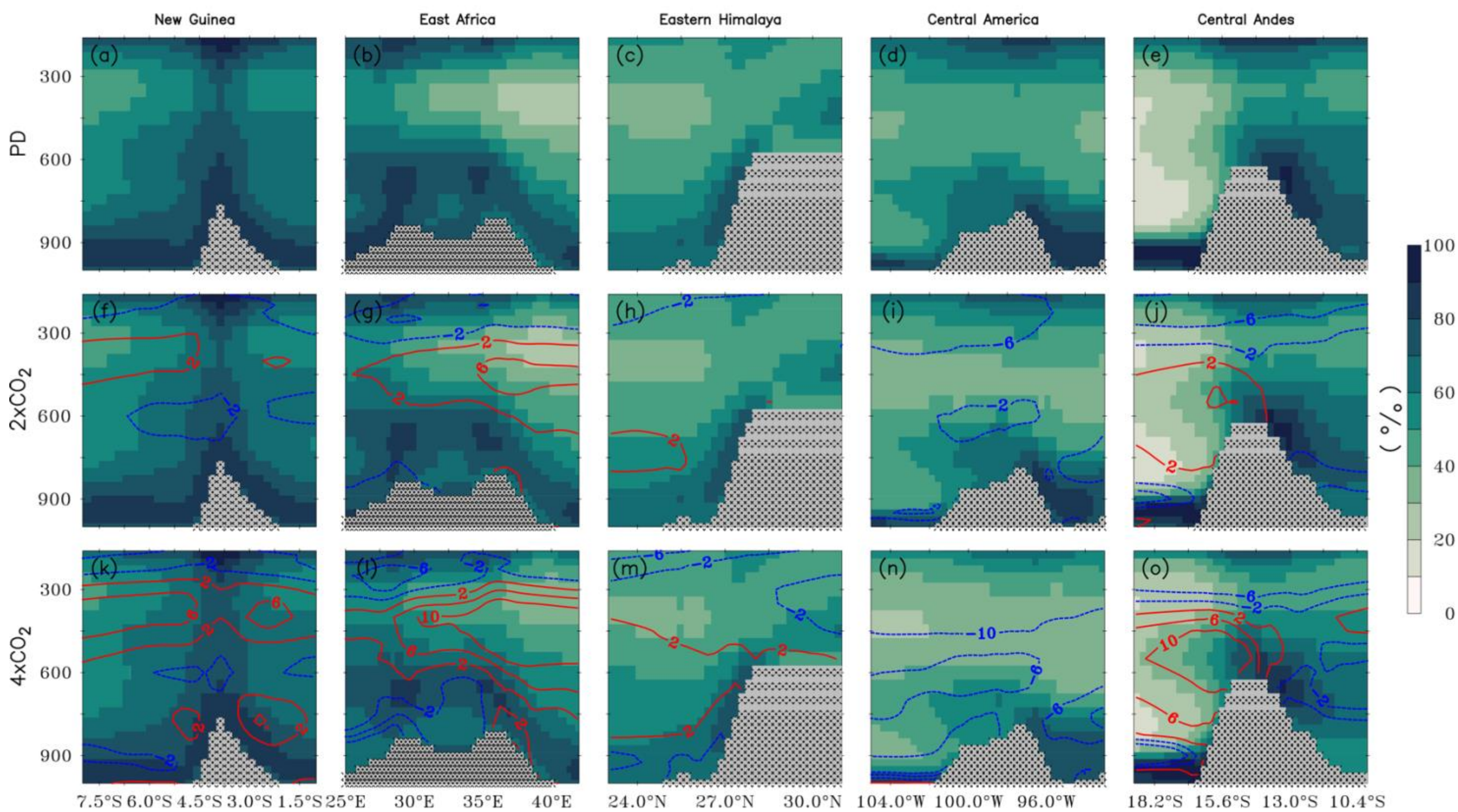

Fig. 2. Vertical structure of relative humidity. Vertical profile of relative humidity (shading) and its anomalies (contour) over New Guinea, East Africa, Eastern Himalaya, Central America, and Central Andes. (a)-(e) For the PD mean state, (f)-(j) for 2×CO_2 mean state, and (k)-(o) for 4×CO_2 mean state respectively. Contours represent relative humidity anomalies due to CO_2 perturbation, where positive values indicate boosts and negative values indicate reduction.

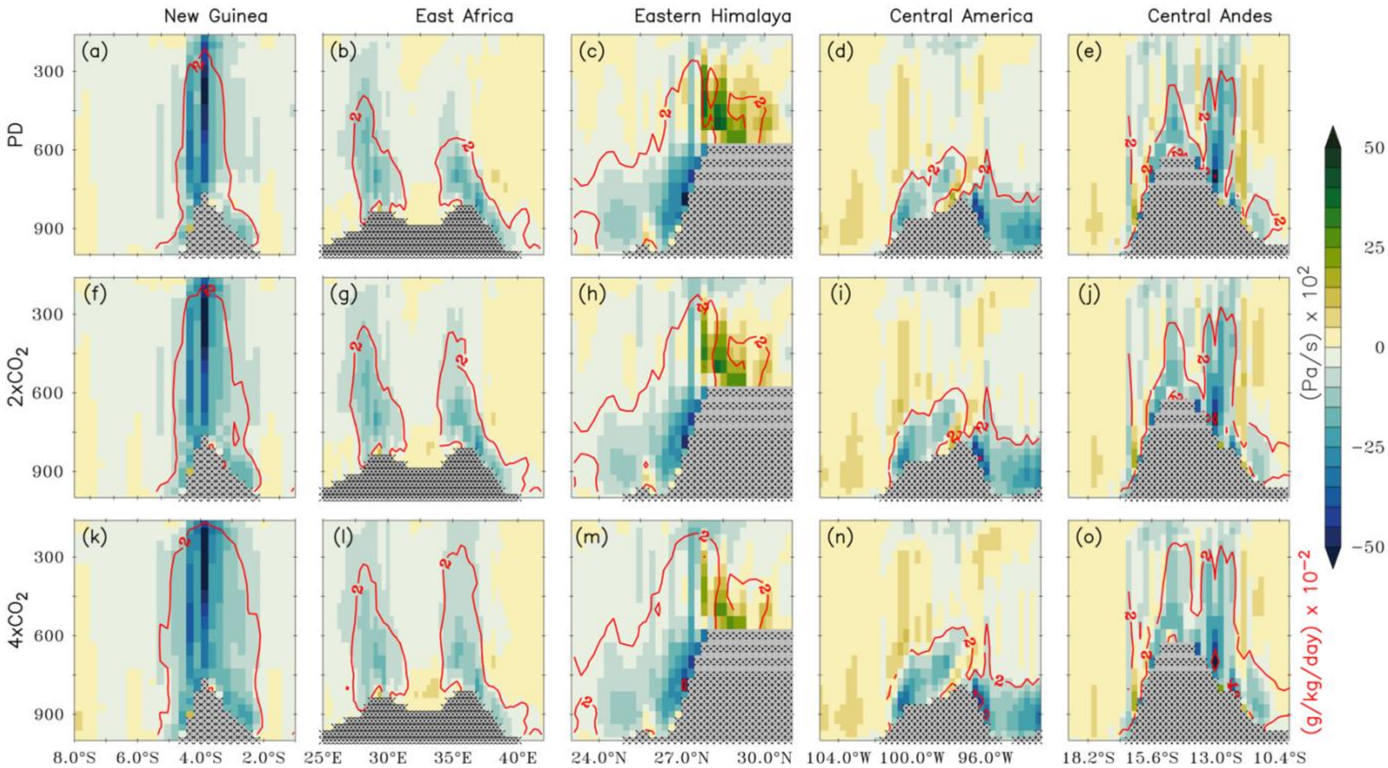

Fig. 3. Vertical structure of vertical velocities with local saturated condensation rate. Vertical profile of mean vertical velocity (shading) and local saturated condensation rate (contour) over New Guinea, East Africa, Eastern Himalaya, Central America, and Central Andes. (a)-(e) PD, (f)-(j) 2×CO_2 experiment, and (k)-(o) 4×CO_2 perturbation experiment respectively. Here, we consider upward motion using the daily scale as precipitation events are associated with upward motions, which offers a clearer idea about ascending motion.

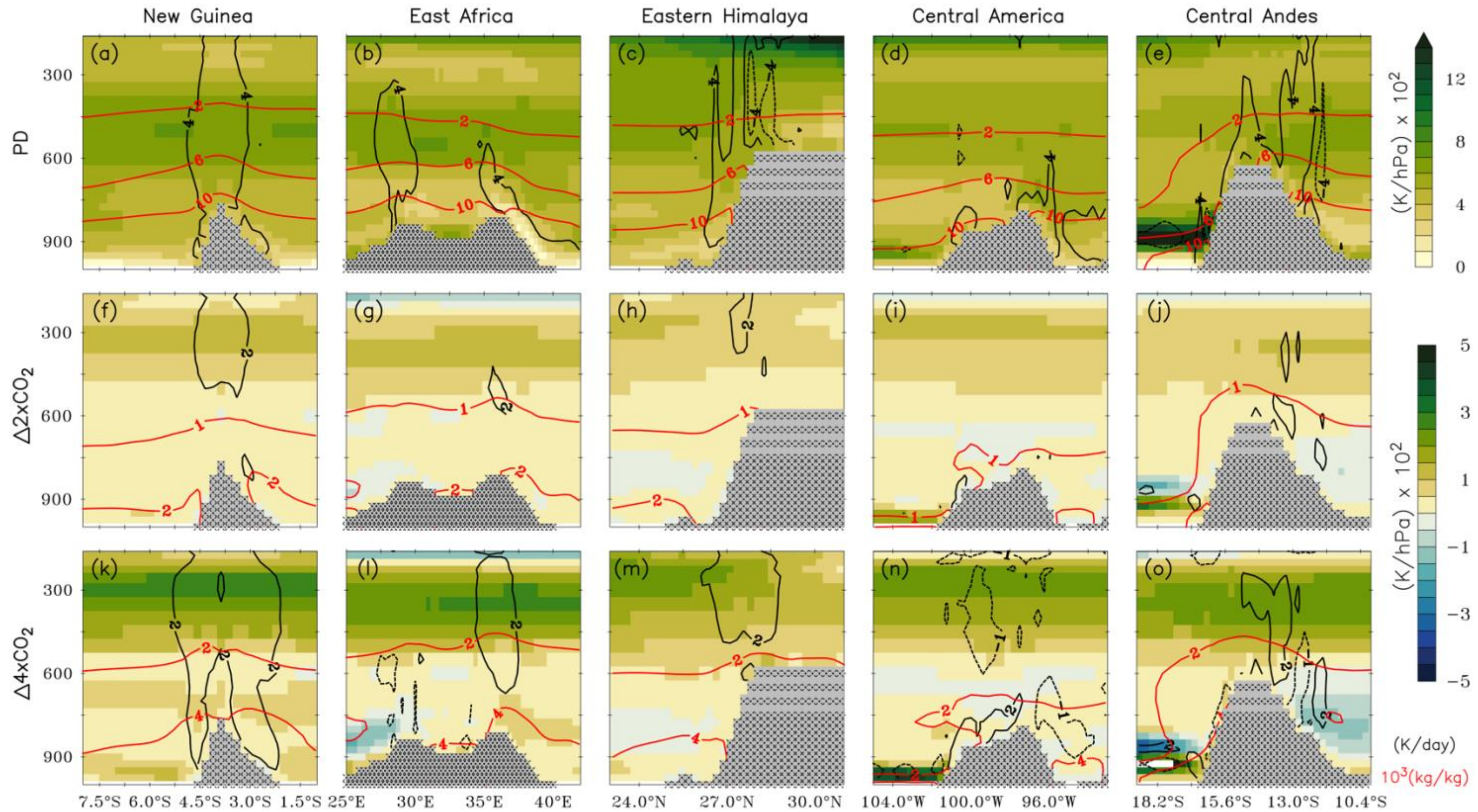

Fig. 4. Vertical structure of thermodynamic condition. Vertical profile of static stability (shading), diabatic heating (black contour) and specific humidity (red contour) over New Guinea, East Africa, Eastern Himalaya, Central America, and Central Andes (a)-(e) for the PD mean state, (f)-(j) for $2\times CO_2$ anomalies, and (k)-(o) for $4\times CO_2$ anomalies respectively.

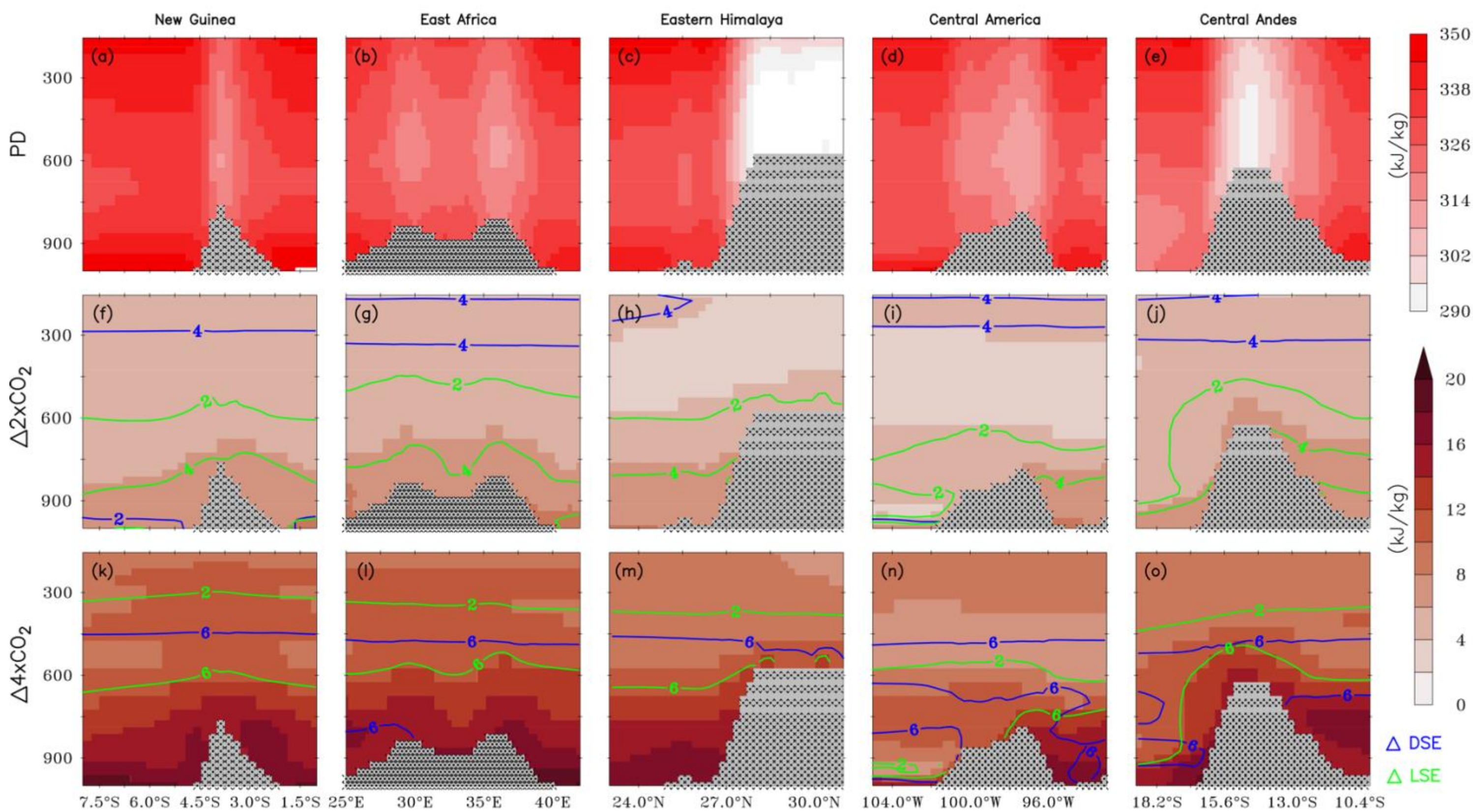

Fig. 5. Vertical structure of moist static energy. Moist static energy (shading) over New Guinea, East Africa, Eastern Himalaya, Central America, and Central Andes for (a)-(e) PD mean state, (f)-(j) $2\times CO_2$ anomalies, and (k)-(o) $4\times CO_2$ anomalies. The green color contour represents changes in latent static energy, and the black color contour represents changes in dry static energy.

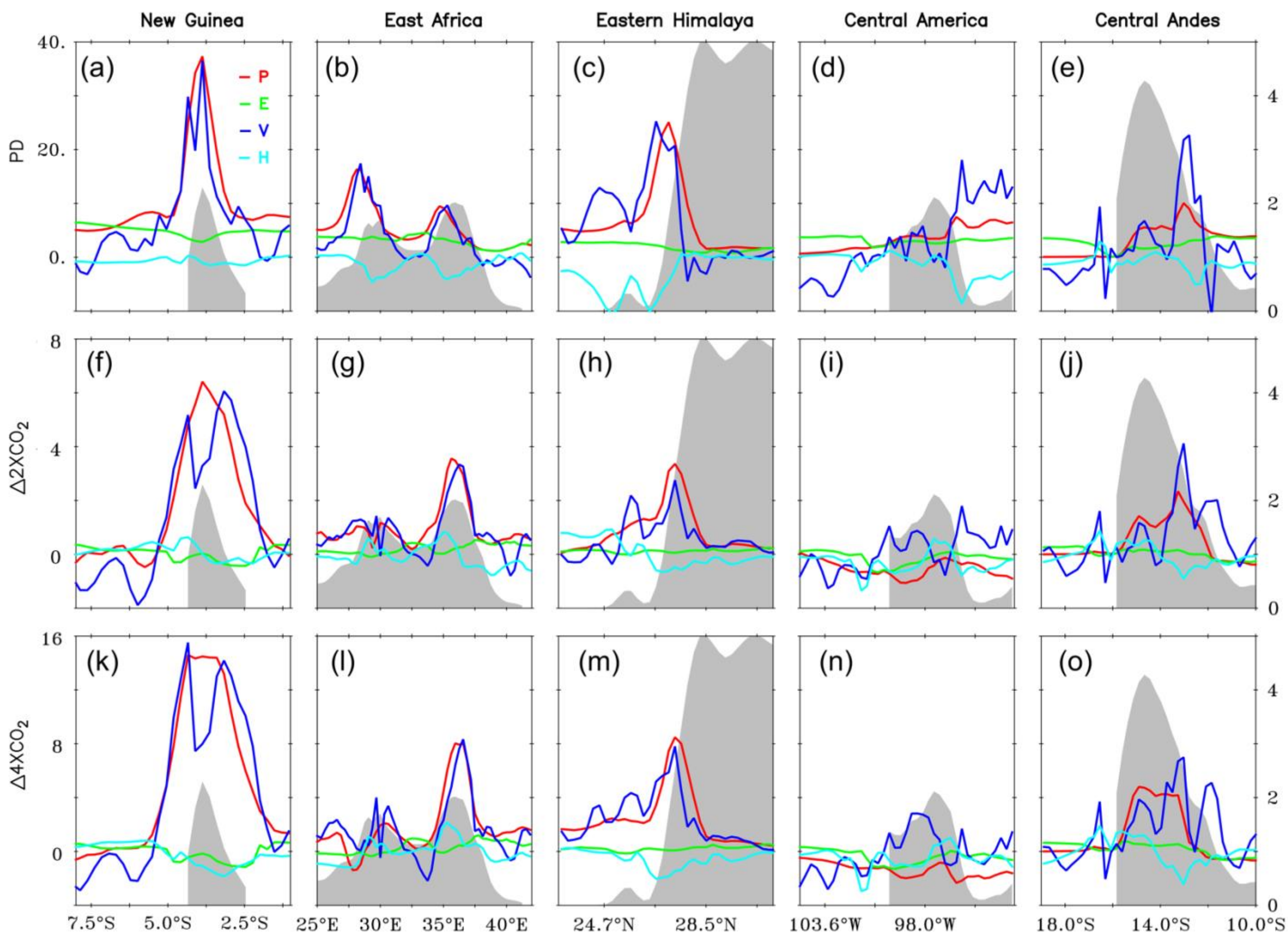

Fig. 6. Moisture budget analysis over selected mountain regions. Cross-section of moisture budget terms (a-e) for PD mean state, (f-j) for 2xCO_2 anomalies, (k-o) 4xCO_2 anomalies respectively. The colored lines indicate the mean state of moisture budget terms; red for precipitation (P), green for evaporation (E), blue for vertical moisture advection (V), and cyan for horizontal moisture advection(H). The shaded grey color represents associated elevation orography.

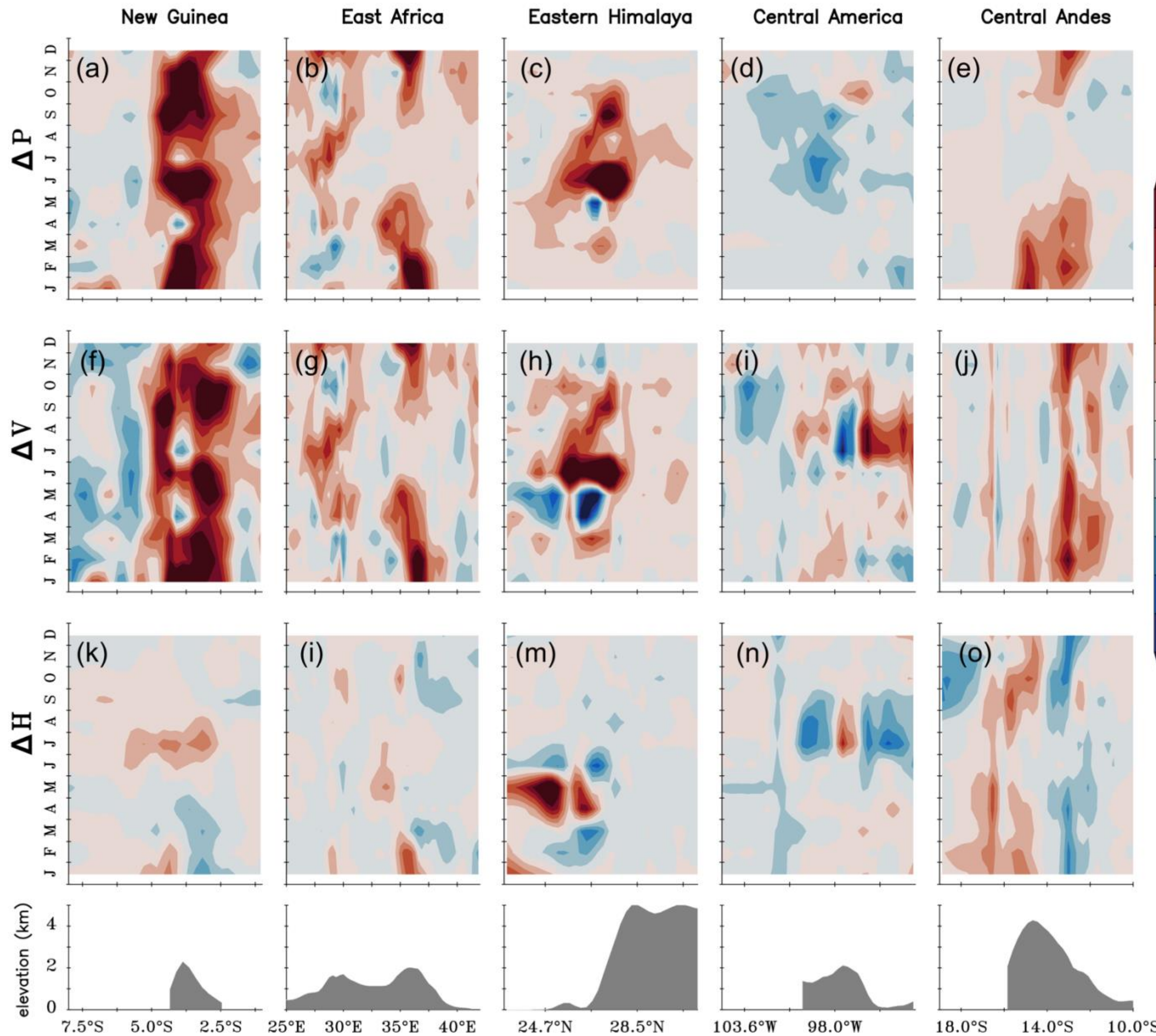

Fig. 7. Seasonal cycle evaluation of dominant terms from moisture budget analysis. Cross-section of moisture budget terms for change in precipitation (P), change in vertical moisture advection (V) and horizontal moisture advection (H) respectively. The shaded grey color in bottom panels represents associated elevation orography.

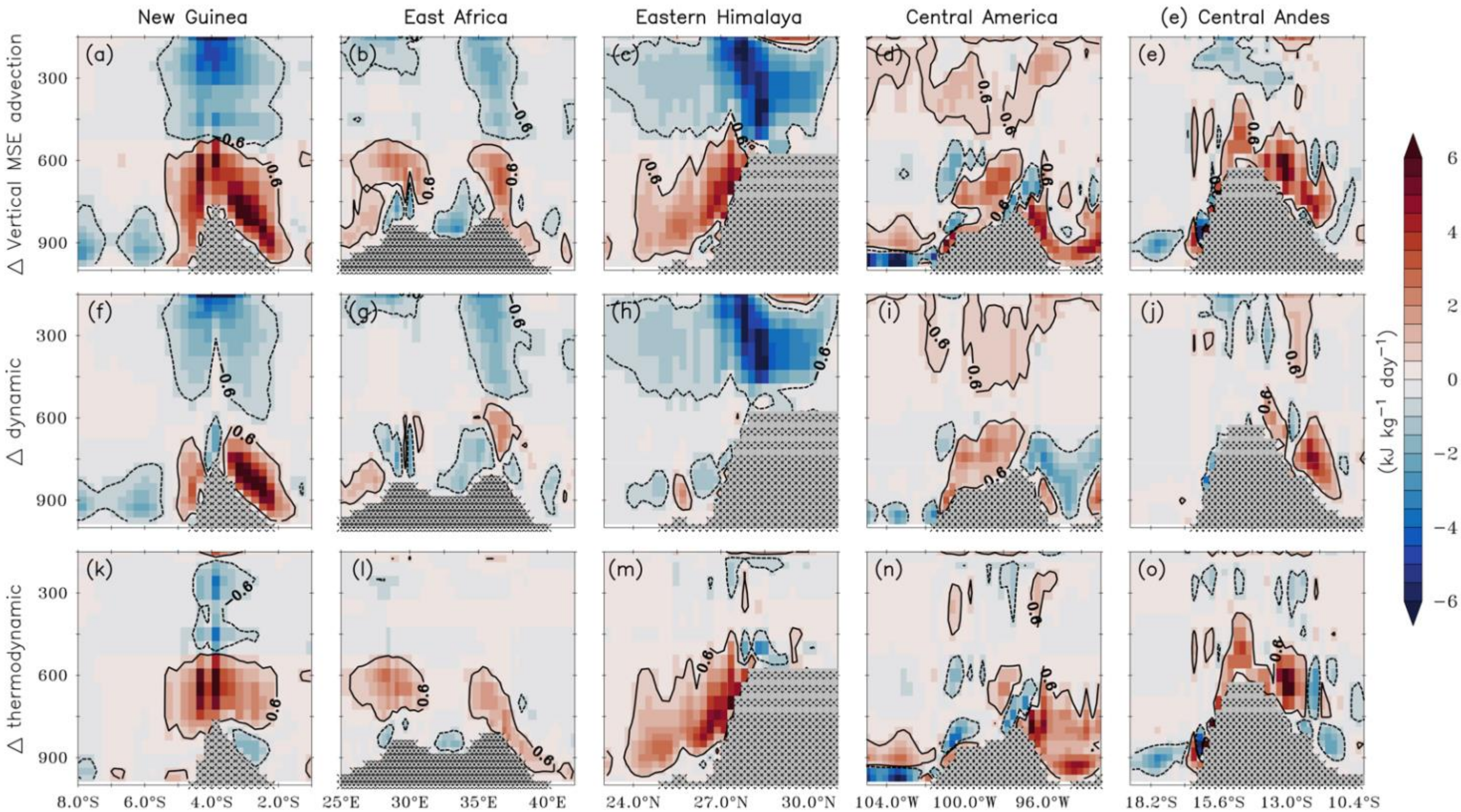

Fig. 8. Vertical structure of anomalous vertical moist static energy (MSE) advection in response to 4xCO_2. Shading and contour denote projected changes in vertical MSE advection over New Guinea, East Africa, Eastern Himalayas, Central America, and Central Andes. (a)-(e) Change in net vertical MSE advection, (f)-(j) change in the dynamical component of vertical MSE advection, and (k)-(o) change in a thermodynamical component of vertical MSE advection, respectively. Positive contours represent energy import and negative energy export.

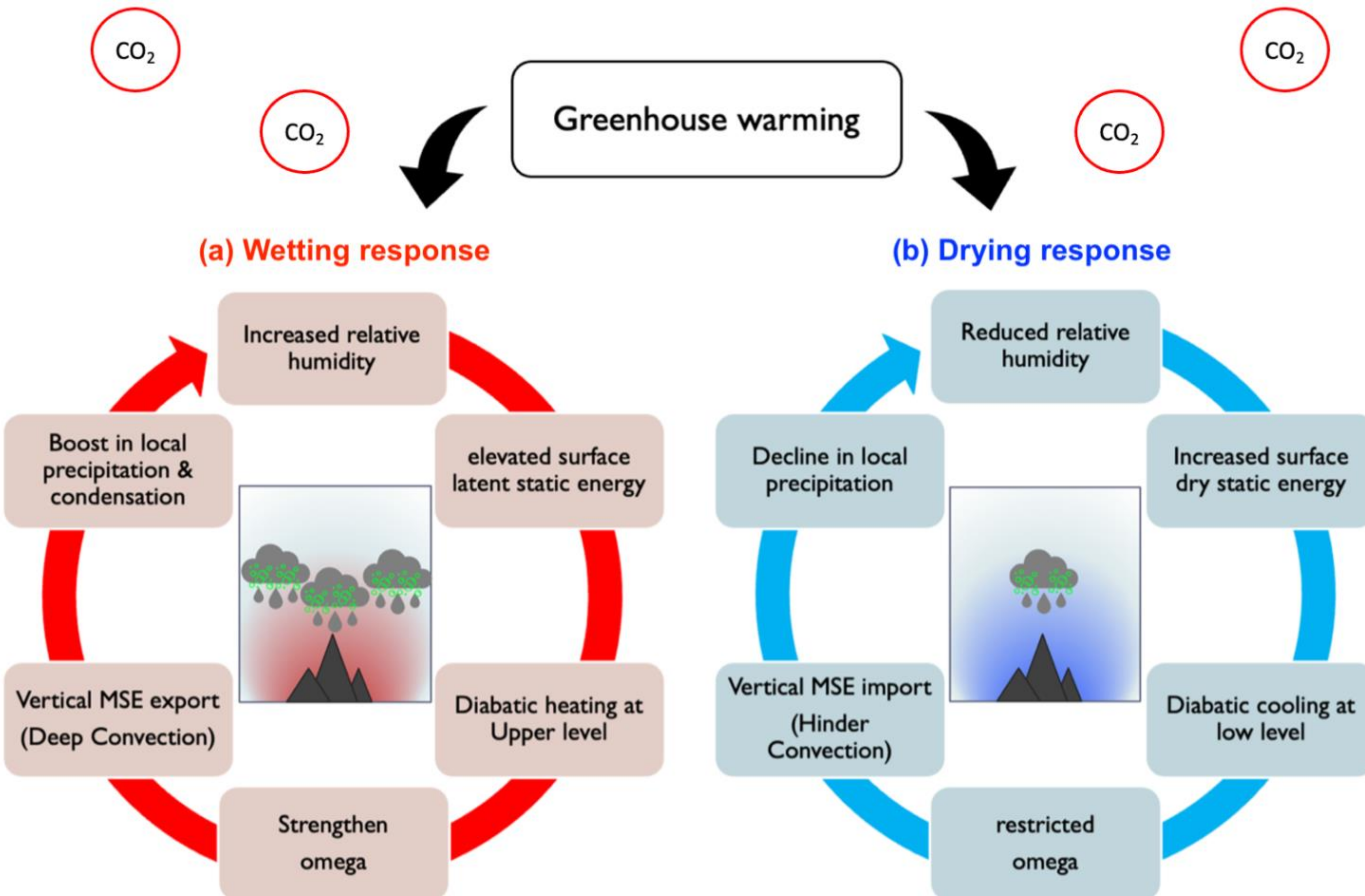

Fig. 9. Schematic representation of "Orographic moist-convection feedback mechanism" over low-latitude mountains.

(a) Wetting response:

Atmospheric relative humidity in the mountain terrain will increase due to greenhouse warming and favors a drop strengthen ascending motion in a humid climate through total diabatic heating. Simultaneously, vertical moist static energy export will feed ascending motion by deep convection. It boosts local precipitation and further contribute to the initial humidity.

(b) Drying response:

Atmospheric relative humidity in the mountain will reduce and this limited humidity weakens ascending motion through total diabatic cooling. Dry static energy contributes to low-level warming and dry conditions. Vertical moist static energy import will feed descending motion. Local precipitation decreases and initial humidity is further reduced as a result.

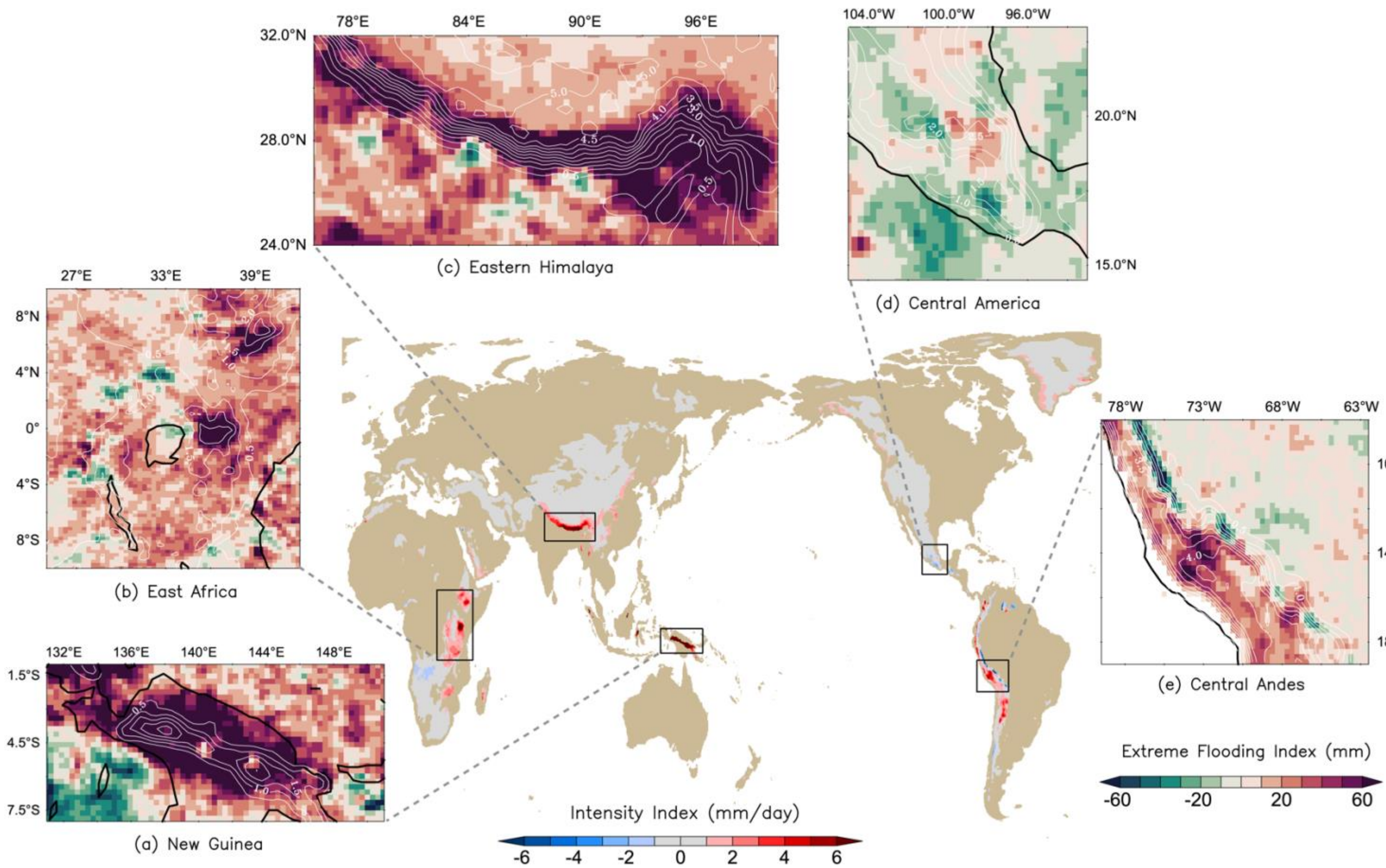

Fig. 10. Projected change in precipitation extremes over global mountain system in response to 4×CO_2. The center panel indicates extreme intensity index (SDII), and sub-panels (a)-(e) show the extreme flooding index (Rx5day). White contour shows an elevation orography of 0.5 km interval.

Earth's Future

Supporting Information for to

Projected Changes in Mountain Precipitation under CO_2-induced warmer climate

Kad et al.

Contents of this file

Supplementary Methods

Temperature lapse rate ($^{o}C\ km^{-1}$)

The atmospheric lapse rate is defined as the temperature changes with height in the atmosphere (from the surface to 100 hPa). It is obtained by least-squares linear regression of temperature to emanate lapse rates.

Moisture advection ($g\ kg^{-1}\ day^{-1}$)

The net moisture advection (Q_{adv}) is a sum of the vertical moisture advection and horizontal moisture advection, using a robust physical framework. The vertical moisture advection can split into its dynamic component related to atmospheric circulation change pattern. The thermodynamic component relates to its change in moisture content controlled by the Clausius-Clapeyron relation.

$$\Delta Q_{adv} = (\Delta V_{dynamic} + \Delta V_{thermodynamic}) + \Delta H$$

$$\Delta Q_{adv} = -\left(\Delta\omega.\frac{\partial\overline{q}}{\partial p}\right) - \left(\overline{\omega}.\frac{\partial\Delta q}{\partial p}\right) - \Delta(V_h.\nabla q)$$

Definition of precipitation extremes

We use the following indices to examine the precipitation extreme events (Calculated over equilibrated last 20 years of each simulation).

Table S1. Precipitation extremes indices (Karl et al., 1999) were used to define extremes events.

Type	**Indices**	**Name**	**Definition**	**Unit**
Absolute	SDII	Simple daily intensity index	Annual precipitation per total number of wet days	mm day^{-1}
	Rx1day	Highest 1-day precipitation	Maximum precipitation in 1-day	mm
	Rx5day	Highest 5-day precipitation	Maximum precipitation within 5-day	mm
Threshold	R10	Heavy rainy days	Number of days when precipitation more or equal to 10mm	day
	R20	Very heavy rainy days	Number of days when precipitation more or equal to 20mm	day

Supplementary Figures

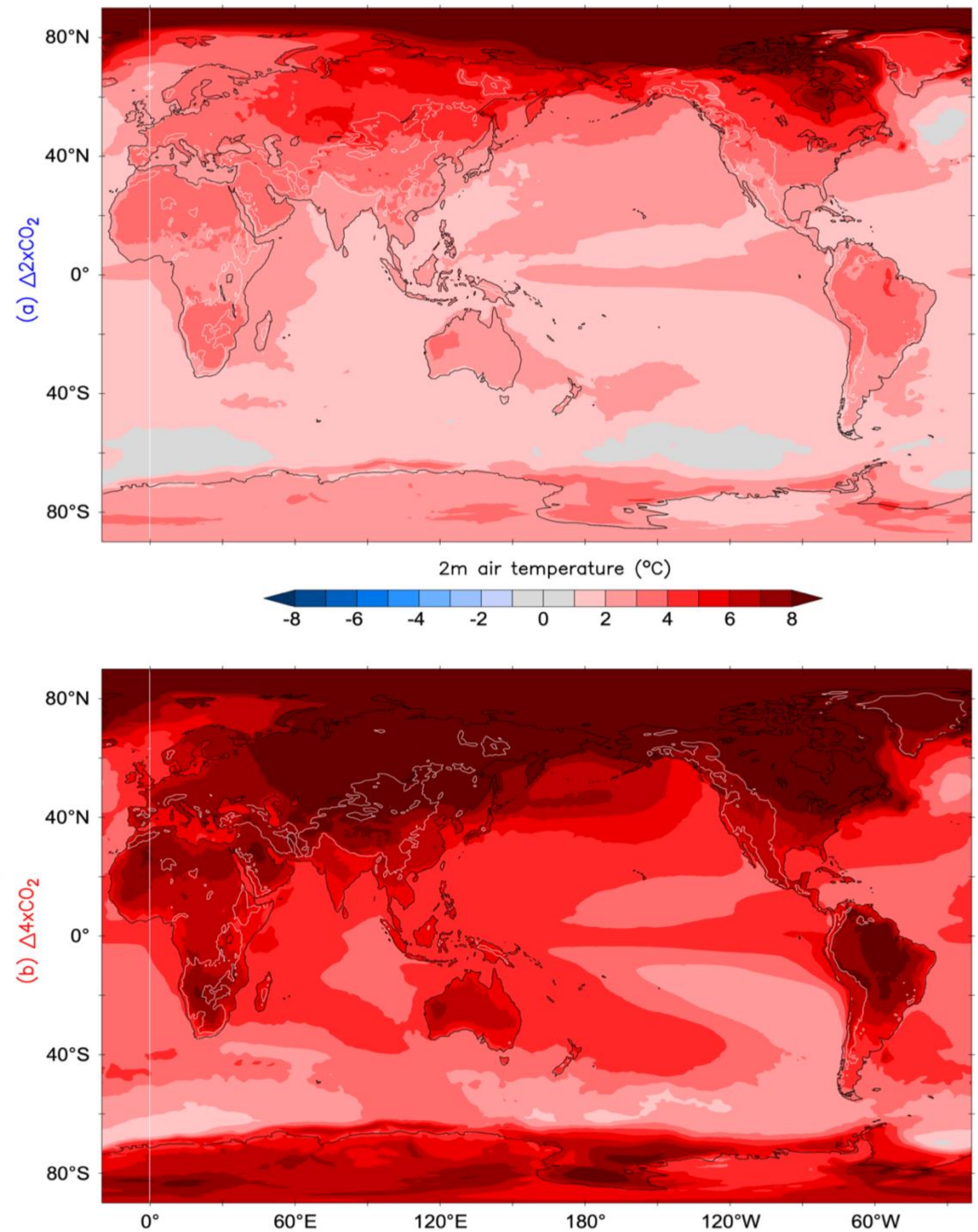

Fig. S1. Global mountain system warming in response to CO_2 perturbation. Change in 2 m air temperature between (a) 2xCO_2 and PD and (b) 4xCO_2 and PD. White contour presents global mountain regions (excluding antarctica) with the elevation is higher than 1km.

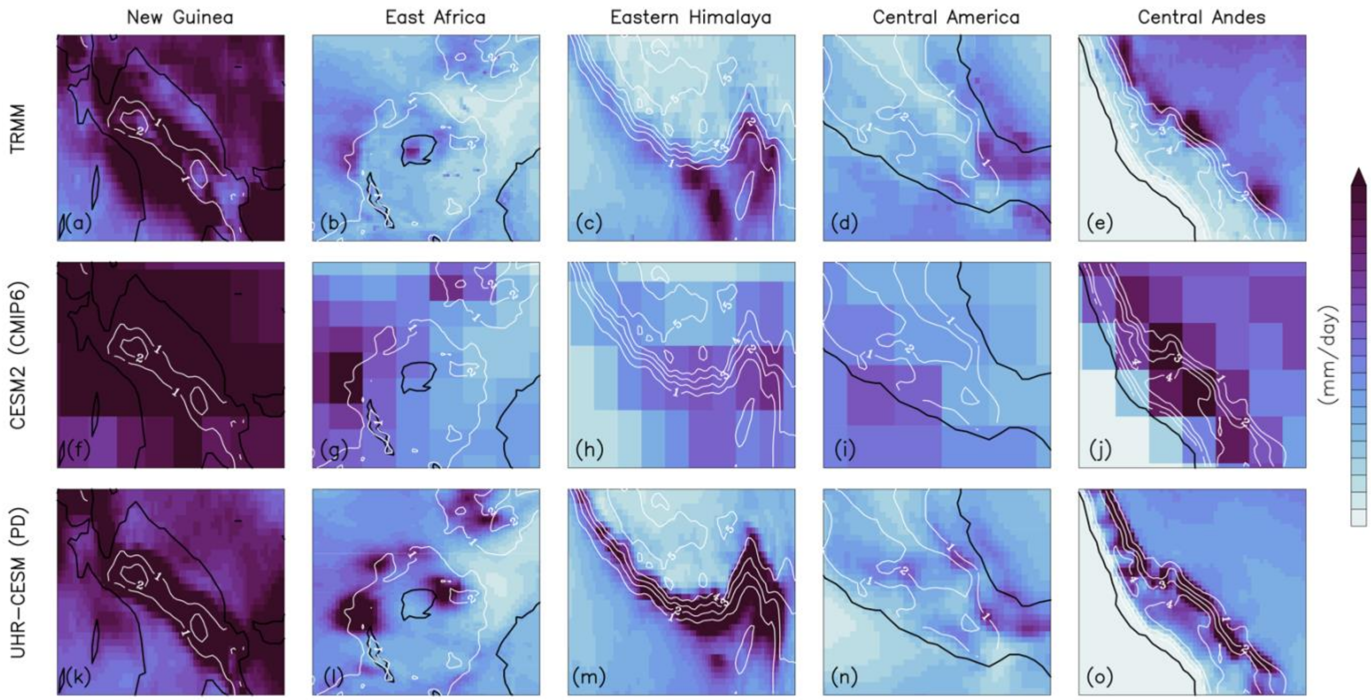

Fig. S2. Annual mean precipitation in observation and model simulation. Annual mean precipitation climatology over chosen mountains from (a-e) satellite product, (f-j) CESM2 simulation having about 100 km nominal resolution, and (k-o) PD simulation having about 25 km resolution from UHR-CESM. The satellite dataset was obtained from the Tropical Rainfall Measurement Mission (TRMM, http://disc.sci.gsfc.nasa.gov/)(Huffman et al., 2010) 3B43 (this data merges the TRMM 3B42 product adjusted with the GPCC rain gauge) during 2000-2019 and the CESM2 model data from Coupled Model Intercomparison Project Phase 6 (CMIP6, https://www.cesm.ucar.edu/projects/CMIP6/)(Danabasoglu et al., 2020) during 1996-2015. The white contour shows an elevation orography of 1 km interval from the UHR-CESM for consistency and comparison.

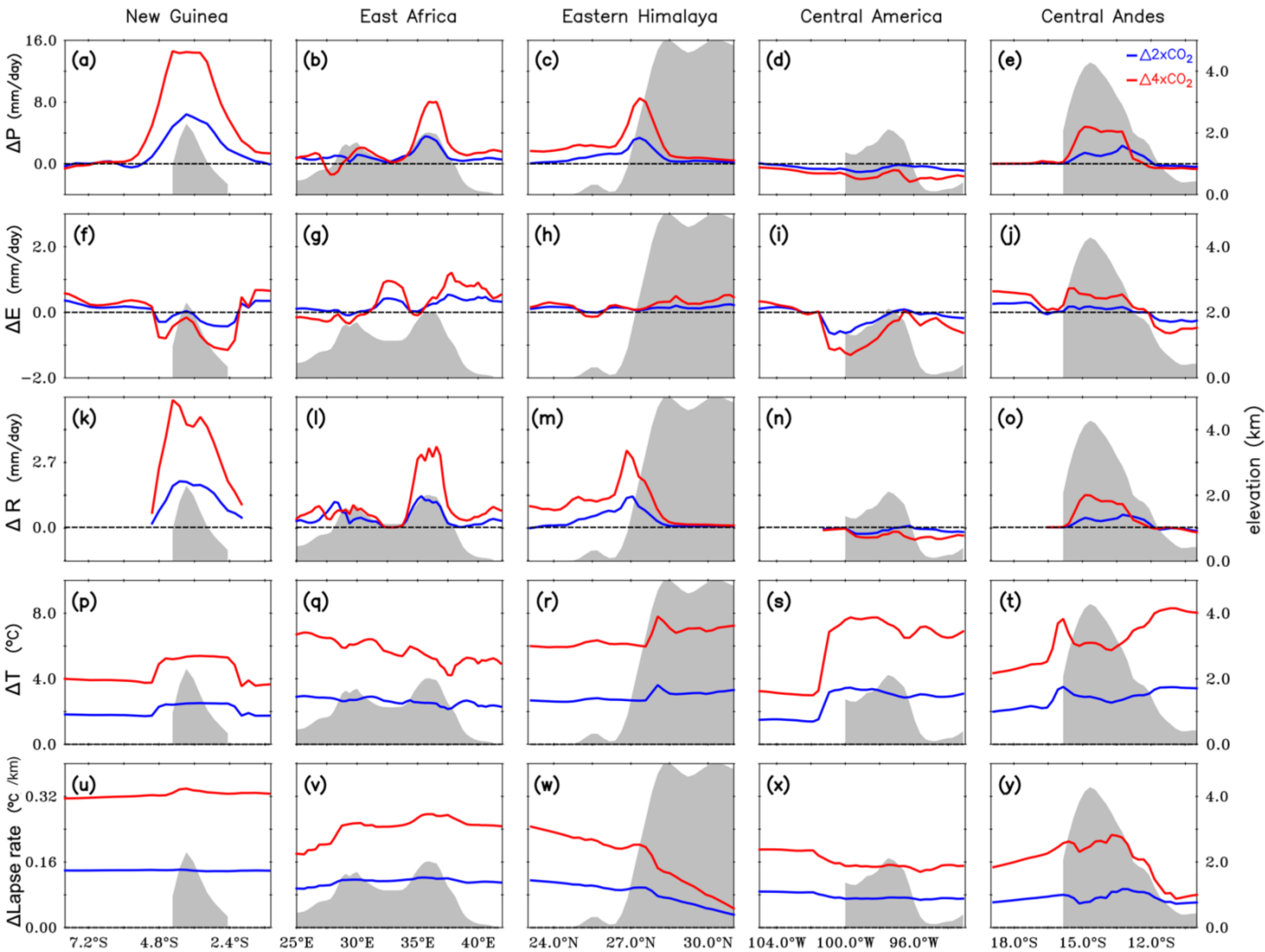

Fig. S3. Changes in various parameters over selected major mountain regions in response to CO_2 perturbation. Cross-section of precipitation (a-e), evaporation at surface (f-j), surface runoff (k-o), temperature (p-t), and lapse rate (u-y). The blue line indicates changes with respect to $2xCO_2$ anomalies, and the red line indicates changes with $4xCO_2$ anomalies. Shaded grey color represents orography.

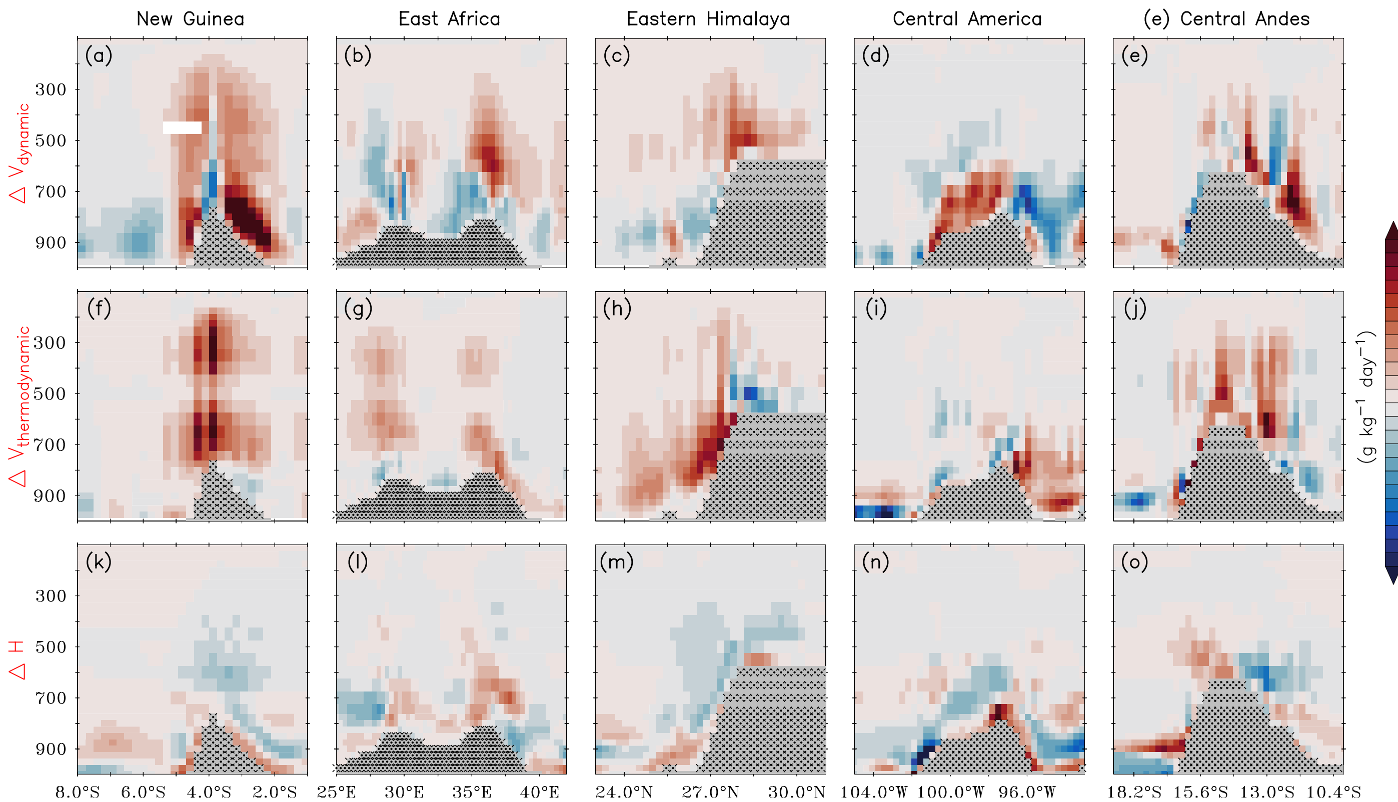

Fig. S4. Vertical structure of anomalous moisture advection in response to 4xCO_2. Shading denotes projected change in moisture advection over New Guinea, East Africa, Eastern Himalayas, Central America, and Central Andes. (a)-(e) Change in vertical dynamic moisture advection, (f)-(j) change in vertical thermodynamic moisture advection, and (k)-(o) change in horizontal moisture advection, respectively.

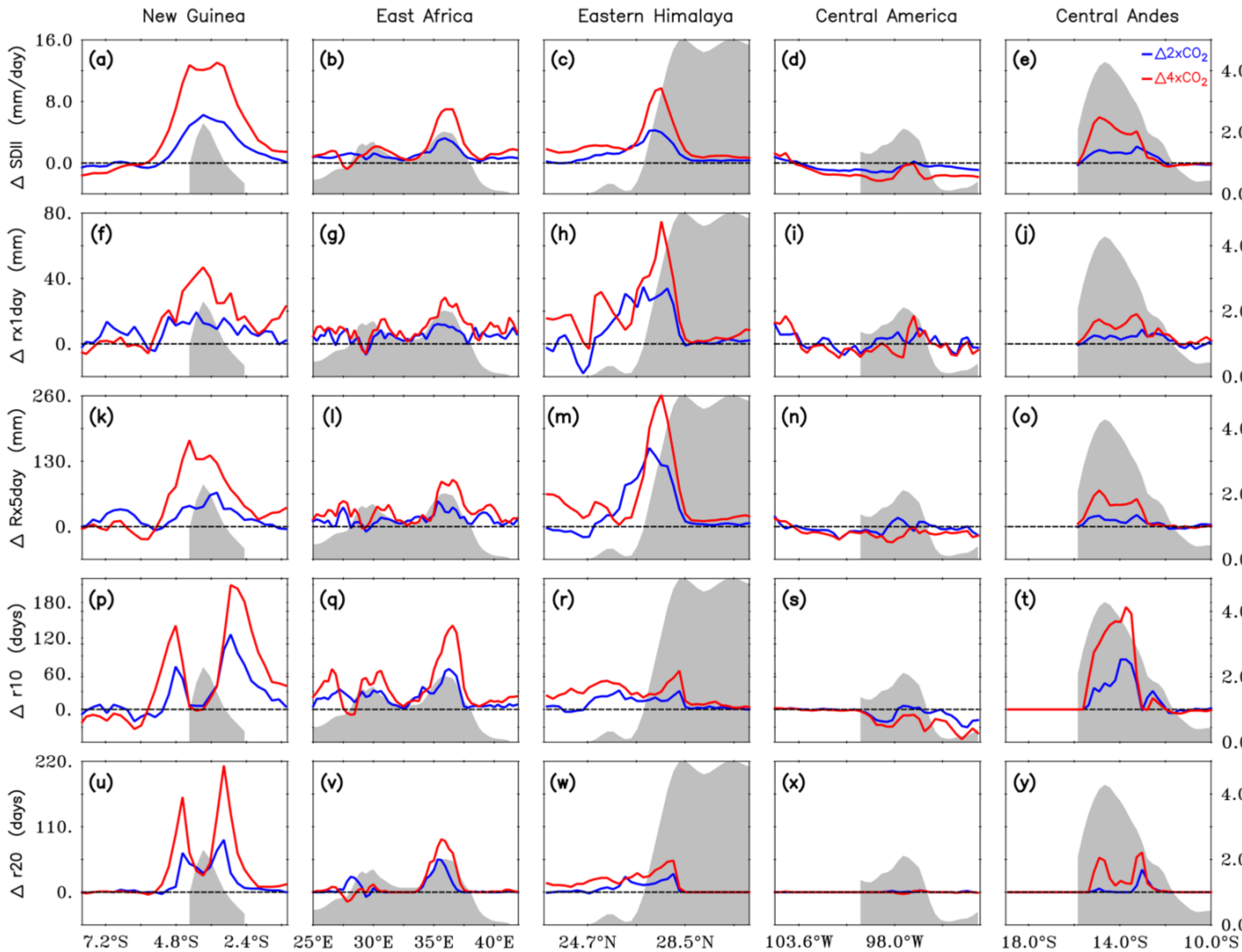

Fig. S5. Changes in various extreme precipitation indices. Cross-section of SDII (a-e), Rx1day (f-j), Rx5day (k-o), R10 (p-t), and R20 (u-y) shown with shaded grey color elevation orography (for more details in supplementary Table 1). The blue line indicates changes with respect to $2xCO_2$ anomalies, and the red line indicates changes with $4xCO_2$ anomalies.

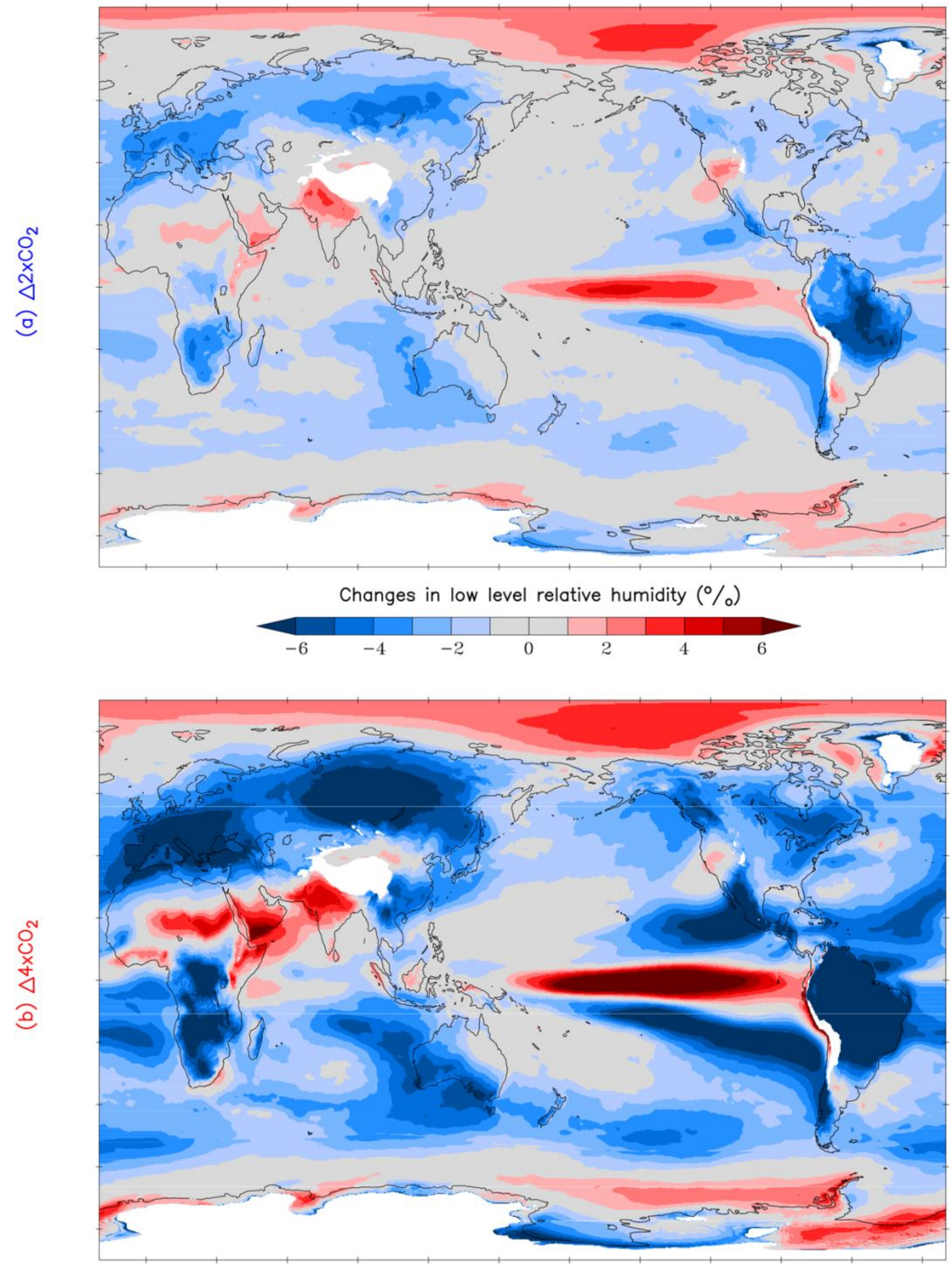

Fig. S6. Relative humidity response to CO_2 perturbation. The low-level relative humidity is defined mean of 750 hPa to 1000 hPa model pressure level.

Supplementary References

Danabasoglu, G., Lamarque, J. F., Bacmeister, J., Bailey, D. A., DuVivier, A. K., Edwards, J., et al. (2020). The Community Earth System Model Version 2 (CESM2). *Journal of Advances in Modeling Earth Systems*, *12*(2). https://doi.org/10.1029/2019MS001916

Huffman, G. J., Adler, R. F., Bolvin, D. T., & Nelkin, E. J. (2010). The TRMM Multi-satellite Precipitation Analysis (TMPA). In *Satellite Rainfall Applications for Surface Hydrology*. https://doi.org/10.1007/978-90-481-2915-7_1

Karl, T. R., Nicholls, N., & Ghazi, A. (1999). CLIVAR/GCOS/WMO Workshop on Indices and Indicators for Climate Extremes - Workshop summary. In *Climatic Change* (Vol. 42). https://doi.org/10.1023/A:1005491526870